OXIDATIVE SIGNAL-INDUCIBLE1 induces immunity by coordinating N-hydroxypipecolic acid, salicylic acid, and camalexin synthesis

Anamika A. Rawat[1]* , Michael Hartmann[2]* , Anne Harzen[3] , Raphael Lugan[4], Sara Christina Stolze[3] , Celine Forzani[5], Laura Abts[2], Sophie Reißenweber[2], Naganand Rayapuram[1] , Hirofumi Nakagami[3] , Jürgen Zeier[2,6] and Heribert Hirt[1,5,7]

[1]Darwin21 Desert Initiative, Biological and Environmental Sciences and Engineering Division, King Abdullah University of Science and Technology (KAUST), Thuwal 23955, Saudi Arabia; [2]Department of Biology, Institute for Molecular Ecophysiology of Plants, Heinrich Heine University, Universitätsstraße 1, Düsseldorf D-40225, Germany; [3]Max Planck Institute for Plant Breeding Research, Cologne D-50829, Germany; [4]UMR Qualisud, Avignon Université, Avignon Cedex 9 84916, France; [5]Department of Plant Molecular Biology, University of Vienna, Dr. Bohrgasse 9, Vienna, 1030, Austria; [6]Cluster of Excellence on Plant Sciences (CEPLAS), Heinrich Heine University, Universitätsstraße 1, Düsseldorf D-40225, Germany; [7]Institute of Plant Sciences Paris-Saclay IPS2, CNRS, INRAe, Université Paris-Sud, Université Evry, Université Paris-Saclay, Bâtiment 630, 91405 Orsay, France

Authors for correspondence:
Jürgen Zeier
Email: juergen.zeier@hhu.de

Heribert Hirt
Email: heribert.hirt@kaust.edu.sa

Summary

- Expression of OXIDATIVE SIGNAL-INDUCIBLE1 (OXI1) is induced by a number of stress conditions and regulates the interaction of plants with pathogenic and beneficial microbes.
- In this work, we generated Arabidopsis OXI1 knockout and genomic OXI1 overexpression lines and show by transcriptome, proteome, and metabolome analysis that OXI1 triggers ALD1, SARD4, and FMO1 expressions to promote the biosynthesis of pipecolic acid (Pip) and N-hydroxypipecolic acid (NHP).
- OXI1 contributes to enhanced immunity by induced SA biosynthesis via CBP60g-induced expression of SID2 and camalexin accumulation via WRKY33-targeted transcription of PAD3. OXI1 regulates genes involved in reactive oxygen species (ROS) generation such as RbohD and RbohF. OXI1 knock out plants show enhanced expression of nuclear and chloroplast genes of photosynthesis and enhanced growth under ambient conditions, while OXI1 overexpressing plants accumulate NHP, SA, camalexin, and ROS and show a gain-of-function (GOF) cell death phenotype and enhanced pathogen resistance. The OXI1 GOF phenotypes are completely suppressed when compromising N-hydroxypipecolic acid (NHP) synthesis in the fmo1 or ald1 background, showing that OXI1 regulation of immunity is mediated via the NHP pathway.
- Overall, these results show that OXI1 plays a key role in basal and effector-triggered plant immunity by regulating defense and programmed cell death via biosynthesis of salicylic acid, N-hydroxypipecolic acid, and camalexin.

Introduction

As sessile organisms, plants have developed various strategies to survive different stresses. Their ability to adapt to changing environments largely relies on sensing and signaling processes, which are based on receptors and signaling networks. Plant plasma membrane-localized pattern-recognition receptors (PRRs) perceive microbe-derived molecular patterns, leading to pattern-triggered immunity (PTI) (Alhoraibi et al., 2019). Pattern-triggered immunity is the first layer of plant immunity and is essential for plants to resist diverse pathogens (DeFalco & Zipfel, 2021). Among the best-known PRRs is FLAGELLIN SENSITIVE2 (FLS2), which perceives a conserved 22-amino acid epitope (flg22) of the N-

terminus of bacterial flagellin (Gómez-Gómez & Boller, 2000). Upon ligand binding, FLS2 interacts with BRASSINOSTEROID INSENSITIVE1-ASSOCIATED KINASE1 (BAK1) to form an active receptor complex (Chinchilla et al., 2007). Within minutes, PRRs trigger downstream responses, including a transient influx of calcium ions from the apoplast, activation of calcium-dependent protein kinases, the production of extracellular reactive oxygen species (ROS), and the activation of mitogen-activated protein kinases (MAPKs) (Ligterink et al., 1997; Jeworutzki et al., 2010; Ranf et al., 2011; Bigeard et al., 2015).

To overcome PTI, pathogens deliver effector proteins into host cells, resulting in effector-triggered susceptibility (ETS). Resistance to pathogens can occur when specific intracellular receptors, called resistance (R) proteins, recognize race-specific avirulence (avr) effectors. Under these conditions, the R proteins

*These authors contributed equally to this work.

activate strong defense reactions, termed effector-triggered immunity (ETI) (Jones & Dangl, 2006). Effector-triggered immunity usually triggers a localized cell death at the infection site, called the hypersensitive response (HR), which restricts pathogen growth (Caplan et al., 2008).

Plant defense comprises PTI and ETI, and a successful defense against pathogens relies on mutual potentiation of immunity by both PTI and ETI components (Pruitt et al., 2021). Pattern-triggered immunity and ETI are associated with the induction of systemic acquired resistance (SAR) in uninfected distal parts of the plant, which provides broad-spectrum resistance against subsequent pathogen challenges (Gruner et al., 2013). The establishment of SAR in response to an inducing pathogen inoculation requires the accumulation and coordinated action of the immune-regulatory metabolites salicylic acid (SA) and N-hydroxypipecolic acid (NHP) (Nawrath & Métraux, 1999; Hartmann et al., 2018; Hartmann & Zeier, 2019; Zeier, 2021). In Arabidopsis, the ISOCHORISMATE SYNTHASE1 (ICS1)-catalyzed conversion of the shikimate pathway intermediate chorismate to isochorismate is a key biochemical event for the pathogen-induced biosynthesis of SA (Wildermuth et al., 2001). ENHANCED DISEASE SUSCEPTIBILITY5 exports isochorismate from the plastid to the cytosol, where the cytosolic amidotransferase avrPphB SUSCEPTIBLE3 (PBS3) conjugates glutamate to isochorismate to produce isochorismate-9-glutamate, which spontaneously decomposes into SA (Rekhter et al., 2019; Torrens-Spence et al., 2019).

N-hydroxypipecolic acid is synthesized through N-hydroxylation of the nonprotein amino acid pipecolic acid (Pip) by flavin-dependent monooxygenase (FMO1) (Chen et al., 2018; Hartmann et al., 2018). Pipecolic acid is derived from L-Lys by consecutive transamination and reduction steps that involve the aminotransferase AGD2-LIKE DEFENSE RESPONSE PROTEIN1 (ALD1) and the reductase SAR-DEFICIENT4 (SARD4), respectively (Návarová et al., 2012; Ding et al., 2016; Hartmann et al., 2017).

The OXIDATIVE SIGNAL-INDUCIBLE1 (OXI1) protein kinase has emerged as a potential player linking the activation of MPK3/6 to disease resistance (Rentel et al., 2004; Petersen et al., 2009). OXIDATIVE SIGNAL-INDUCIBLE1 (OXI1) also plays a role in coordinating the beneficial interaction with the fungus Piriformospora indica (Camehl et al., 2011). Interestingly, OXI1 is regulated transcriptionally and at the protein kinase level by hydrogen peroxide (H_2O_2) (Rentel et al., 2004). Reactive oxygen species of plants are either by-products of photosynthesis or are induced during abiotic stresses and pathogen attack. Among the different forms of ROS, plants produce singlet oxygen ($^1O_2$), superoxide radicals (O_2^-), or H_2O_2 (Apel & Hirt, 2004). Whereas superoxide can spontaneously or enzymatically convert to H_2O_2 and hydroxyl radicals in the presence of metals, the production of these ROS can also increase under stress conditions when the absorbed light energy supersedes the amount of useful energy passing through the photosynthetic electron transport chain. Under these conditions, OXI1 regulates high light-induced programmed cell death via singlet oxygen signaling (Beaugelin et al., 2019).

Major advances in understanding ROS-producing enzymes, ROS sensing as well as compartmentalization and systemic ROS signaling have recently been made (Waszczak et al., 2018; Castro et al., 2021). In this study, we show that OXI1 plays an important role in regulating the trade-off between plant growth and defense. Using transcriptomics, proteomics and metabolomics analyses, we provide evidence that OXI1 is a negative regulator of photosynthesis, but positively regulates biosynthesis of key defense factors, ROS, and camalexin. Importantly, we show that OXI1 regulates various steps in the biosynthesis of NHP and SA, the two key regulators of SAR. Accordingly, OXI1 knockout and overexpressor plants show opposite behavior in plant growth and both basal and ETI. Taken together, our study shows that OXI1 coordinates plant defense responses and growth.

Materials and Methods

Plant material and growth conditions

Arabidopsis thaliana Columbia (Col-0) was used as wild-type (WT) in this study. The 2.2 kb OXI1 promoter and the genomic sequence of OXI1 with the 5′ UTR and 3′ UTR were amplified by polymerase chain reaction (PCR) and cloned into pCambia 3300 carrying BASTA resistance (Forzani et al., 2011). The HA tag was cloned at the Sal I site found at the ATG site of OXI1. The construct was used to transform Col-0 oxi1-2 (Gabi_355H08) using the floral dip method and analyzed by qRT-PCR and immunoblotting with HA antibody. For OXI1 expression analysis, an OXI1::GUS line was used (Forzani et al., 2011).

Arabidopsis plants were grown individually in Jiffy-7 pellet in a controlled cultivation chamber with a 12 h : 12 h, light : dark at 110 µmol m^{-2} s^{-1} light intensity and a relative humidity of 60%. Day and night temperatures were set to 22°C and 20°C, respectively. Nonflowering 5-wk-old plants were used for bacterial disease assay and ROS burst assay. For microarray analysis of seedlings, surface-sterilized seeds were vernalized at 4°C in the dark for 3 d and then germinated on 1/2 strength Murashige and Skoog (1/2MS, M6899; Sigma) plates, containing 0.5% sucrose (S5016; Sigma), 1% agar (A1296; Sigma), and 0.5% MES (M8250; Sigma), grown at 23°C, 60% humidity, and 125 µmol m^{-2} s^{-1} light intensity with a 16 h : 8 h, light : dark photoperiod. The plants were transferred to a new 60 mm × 60 mm Petri dish with 10 ml 1/2MS medium overnight before treatment.

Immunoblotting

Immunoblotting was carried out as described (Frei dit Frey et al., 2014). Briefly, 10 µg of total protein extracts from roots was denatured with SDS loading buffer and then separated by 8% SDS/PAGE before transfer to polyvinylidene difluoride membranes (Millipore) by electroblotting. Membranes were probed with Ponceau S (P3504; Sigma) and anti-HA IgG (Covance Carnegie Center, Princeton, NJ, USA). Membranes were developed by enhanced chemiluminescence, as recommended by the manufacturer (GeneImage; Amersham Biosciences).

Pathogen infection assays

Spray and injection infections with *Pst DC3000* and *Pst DC3000 AvrRpm1* (kindly supplied by J. Parker; MPI, Cologne, Germany) and determination of bacterial titers were performed on 4- to 5-wk-old plants as previously described (Berriri *et al.*, 2012). Spray inoculations were performed with bacterial suspensions at 10^8 CFU ml^{-1} in 10 mM MgCl2 with 0.04% Silwet L-77. Infiltration experiments were performed with bacterial suspensions at 10^5 CFU ml^{-1} in 10 mM MgCl$_2$. At least four plants of each genotype were used per experiment, and the experiments were repeated at least three times. Bacterial numbers in mutant or transgenic lines were compared with Col-0 using a two-tailed Student's *t*-test. *Hyaloperonospora arabidopsidis* isolate *Emwa1* (kindly supplied by J. Parker, MPI) was inoculated onto 2-wk-old seedlings at 5×10^4 spores ml^{-1} as previously described (Berriri *et al.*, 2012). To assess plant cell death and *H. arabidopsidis* infection structures, trypan blue staining of the leaves was performed 6-d postinoculation (dpi). Experiments were repeated three times with similar results. Salicylic acid contents were determined after bacterial spray inoculation as previously described (Berriri *et al.*, 2012). For *Pseudomonas syringae* pv *maculicola* strain ES4326 (*Psm*) carrying the *Photorhabdus luminescens* luxCDABE (lux) operon (*Psm lux*) (Zeier *et al.*, 2004; Fan *et al.*, 2008), bacteria were grown in King's B medium supplemented with the appropriate antibiotics at 28°C under constant shaking. Overnight log-phase cultures were washed four times with 10 mM MgCl$_2$ solution and diluted to different final OD$_{600}$ levels for leaf inoculation. The diluted bacterial solutions were pressure-infiltrated from the abaxial side of the leaves using a needleless syringe, covering the whole surface of the respective leaf. To assess bacterial growth in naïve 5-wk-old plants (basal resistance), three fully grown leaves per plant (Berriri *et al.*, 2012) were infiltrated with a suspension of *Psm* lux at OD$_{600}$ = 0.001 between 10:00 h and 11:00 h. At 60 h, the bacterial growth in the infiltrated leaves was determined by measuring the bacterial bioluminescence in leaf disks as described (Hartmann *et al.*, 2018).

Histochemical staining

For studying *OXI1* expression, an *OXI1*::GUS line was used (Forzani *et al.*, 2011). Plant tissues were fixed in 90% acetone for 30 min at 4°C, washed three times with 50 mM sodium phosphate buffer (pH 7.0), and subsequently stained for up to 16 h in 50 mM sodium phosphate buffer (pH 7.0), 2 mM K3Fe(CN6), 2 mM K4Fe(CN6) containing 1 mM 5-bromo-4-chloro-3-indolyl-D-glucuronide (Duchefa, Haarlem, the Netherlands). Tissues were cleared in ethanol and visualized with a stereo microscope (MZ16FA; Leica).

To determine H$_2$O$_2$ accumulation, 5-wk-old plants grown on jiffy pellets in plant growth chambers (Percival Scientific, Perry, IA, USA) under 16 h : 8 h, light : dark photoperiod at 22°C, 60% humidity, were used. The leaves were gently vacuum-infiltrated with 1 mg ml^{-1} DAB in water (D8001; Sigma-Aldrich), and incubated in the dark for 4–5 h at 22°C on a shaker at 80–100 rpm. Following incubation, the samples were destained in bleaching solution (ethanol : acetic acid : glycerol, 3 : 1 : 1). Destained leaves were mounted on microscopic glass slides in 30% glycerol and pictured using Canon EOS 6D.

For cell death staining, detached leaves were treated with trypan blue (1 mg ml^{-1}) according to Beaugelin *et al.* (2019). The trypan blue solution was prepared by dissolving 40 mg trypan blue in 10 ml lactic acid (85%, w/w), 10 ml phenol (buffer equilibrated, pH 7.5–8.0), 10 ml glycerol, and 10 ml distilled water. Leaves were incubated in the trypan blue solution for 40 min, then immediately rinsed with ethanol and washed overnight in ethanol.

GC–MS metabolomics

The metabolomics study was performed on samples from two independent experiments, each including four biological replicates (Methods S1; Table S1). Semiautomated integration of chromatograms was performed with QUANLYNX software (Waters, Milford, MA, USA) after conversion of the raw data into NetCDF format. A model ion was chosen manually to perform a correct integration for 42 peaks, with the following criteria: Gaussian shape, high relative abundance in the mass spectrum, and the absence of saturation in any sample (Table S1). Metabolites were annotated with confidence levels according to the Chemical Analysis Working Group (Sumner *et al.*, 2007), on the basis of both spectral and retention index matches with public database (Kopka *et al.*, 2005). Peak surfaces were then normalized according to the internal standard peak surface (ribitol) and sample fresh weight (FW) (Table S2). Raw metabolomics dataset (accession number MSV000090447) can be downloaded from the publicly available MassIVE repository at the UCSD Center for Computational Mass Spectrometry website: https://massive.ucsd.edu/.

Quantification of defense metabolites

The levels of camalexin, SA, SAG, SGE, Pip, and NHP were determined by gas chromatography/mass spectrometry (GC–MS)-based analyses of plant extracts as detailed in Hartmann *et al.* (2018) and Stahl *et al.* (2019). Briefly, three leaves per plant were inoculated with a suspension of Psm at OD$_{600}$ = 0.005, and control plants were mock-infiltrated with a 10 mM MgCl$_2$ solution. Leaves from one plant were harvested at 10-, 20-, and 48-h postinfection (hpi) after treatment, pooled for one biological replicate, and frozen in liquid nitrogen. Fifty milligrams of pulverized, frozen tissue samples was extracted twice with 1 ml of MeOH : H$_2$O (80 : 20, v/v). For internal standardization, 1 μg of D$_4$-SA, D$_9$-Pip, D$_9$-NHP, indole-3-propionic acid (IPA), and salicin were added. Six hundred micoliters of the extract was evaporated to dryness, and free hydroxyl groups of the analytes were converted into their trimethylsilyl derivatives by adding 20 μl of pyridine, 20 μl of N-methyl-N-trimethylsilyltrifluoroacetamide (MSTFA) containing 1% trimethylchlorosilane (v/v) and 60 μl of hexane and heating the mixture to 70°C for 30 min. The cooled samples were transferred to a GC vial and diluted fivefold with hexane. Two microliters of the sample mixture was separated on a gas chromatograph (GC 7890A; Agilent Technologies, Santa Clara, CA, USA) equipped with a Phenomenex ZB-35 (30 m × 0.25 mm × 0.25 μm)

New
Phytologist

capillary column using the following temperature program: 70°C for 2 min, with 10°C min^{-1} to 320°C, and 320°C for 5 min. Mass spectra were recorded with a 5975C mass spectrometric detector (Agilent Technologies) between m/z 50 and m/z 750 in the electron ionization (EI) mode. Metabolites were quantified by integrating peaks of selected ion chromatograms using MSD CHEMSTATION software v.E.02.01.1177 (Agilent Technologies): SA (m/z 267) relative to D$_4$-SA (m/z 271), Pip (m/z 156) relative to D$_9$-Pip (m/z 165), NHP (m/z 172) relative to D$_9$-NHP (m/z 181), camalexin (m/z 272) relative to IPA (m/z 202), and SAG (m/z 267) and SGE (m/z 193), both relative to salicin (m/z 268).

RNA extraction and qRT-PCR analysis

Total RNA was extracted from 4-wk-old plants grown on jiffy pellets in plant growth chambers (Percival Scientific) under 16 h : 8 h, light : dark photoperiod at 22°C, 60% humidity, using NUCLEOSPIN Plant RNA (Macherey Nagel, Düren, Germany) kit following the manufacturer's protocol. First-strand cDNA was synthesized from 1.5 μg of total RNA using Super-Script III First-Strand Synthesis SUPERMIX kit (Invitrogen). The diluted cDNA (10 times) was used to perform quantitative RT-PCR (qRT-PCR) using SsoAdvanced Universal SYBR Green Supermix (Bio-Rad) on StepOnePlus Real-Time PCR System (Applied Biosystems, Waltham, MA, USA). The data were analyzed using Bio-Rad CFX MANAGER software. ACTIN was used as a housekeeping gene for normalization of gene expression levels. Analyses were performed in triplicate and was repeated thrice with independent RNA samples. Primers used in this study are listed in Table S3.

Transcriptome analysis

Four-week-old plants were collected for RNA analysis. Microarray analysis was carried out using the CATMAV.6.2 array based on Roche-Nimble Gene technology as described (Frei dit Frey et al., 2014). The arrays contained 219 684 primers representing all the Arabidopsis thaliana genes: 37 309 probes corresponding to TAIRv.8 annotation (including 476 probes of mitochondrial and chloroplast genes); 1796 probes corresponding to EUGENE software predictions and 5328 probes corresponding to repeat elements; 1322 probes for miRNA/MIR, 329 probes for other RNAs (rRNA, tRNA, snRNA, and soRNA); and several controls. Three independent biological replicates of the microarray analysis were performed (Table S4). For each biological repetition, 5-wk-old plants grown under 16 h : 8 h, light : dark photoperiod at 22°C, 60% humidity, were collected, and RNA samples were obtained by pooling more than 50 plants. Total RNA was extracted using Qiagen RNAeasy according to the supplier's instructions. For each comparison, one technical replicate with fluorochrome reversal was performed for each biological replicate (six hybridizations per comparison, RIN score cutoff = 7). The labeling of cRNAs withCy3-dUTP or Cy5-dUTP (Perkin-Elmer-NEN Life Science Products, Waltham, MA, USA) and the hybridization to the slides were performed as previously described (Lurin et al., 2004). Two-micron scanning was performed with InnoScan900 scanner (InnopsysR, Carbonne,

France), and raw data were extracted using MAPIXR software (InnopsysR).

Transcriptome analysis was performed as described (Frei dit Frey et al., 2014). Briefly, for each array, the raw data comprised the logarithm of median feature pixel intensity at wavelengths 635 nm (red) and 532 nm (green). For each array, a global intensity-dependent normalization, using LOESS (Locally reweighted Scatter Plot Smoothing), was performed to correct the dye bias. The differential analysis was based on the log ratios averaging over the duplicate probes and over the technical replicates. Hence, the numbers of available data for each gene equal the number of biological replicates and are used to calculate the moderated t-test. Under the null hypothesis, no evidence that the specific variances vary between probes is highlighted by limma (Ritchie et al., 2015), and consequently the moderated t-statistic is assumed to follow a standard normal distribution. To control the false discovery rate, we calculated adjusted P values using the optimized FDR approach (Storey & Tibshirani, 2003). We considered as being differentially expressed the probes with an adjusted P value ≤ 0.05. Analysis was made with the R software. The function SqueezeVar of the library LIMMA was used to smooth the specific variances by computing empirical Bayes posterior means. The library KERFDR was used to calculate the adjusted P-values. The analysis to find overrepresented categories in the gene sets was obtained with AMIGO (Carbon et al., 2008), which is based on a hypergeometric test.

Results

OXI1 overexpression results in a gain-of-function phenotype induces ROS and leaf cell death in late development

Most of the functional analysis of OXI1 was made so far in the Arabidopsis Wassilewskija (Ws) background, hindering a genetic analysis with a large set of available mutants such as in the Columbia accession. Moreover, constitutive OXI1 overexpression function was studied using the strong constitutive 35S cauliflower mosaic virus promoter (Petersen et al., 2009). For these reasons, we generated a set of pOXI1::HA-OXI1 transgenic lines in the Col-0 oxi1-2 background (Beaugelin et al., 2019). Some OXI1 lines were slightly smaller than WT and started to show a gain-of-function (GOF) leaf cell death phenotype after 4 wk of development (Figs 1a, S1). Western blot analysis of these lines showed elevated expression levels (OE1 and OE2), whereas other lines (C1 and C2) resembled WT plants and showed low expression levels (Fig. 1b). C1 and C2 were therefore considered as complementation lines. The cell death phenotype in the OXI1-OE lines consistently started with the darkening of the center of the rosettes, which then spread to the petioles and the leaves. The pattern of cell death development parallels the expression pattern of OXI1 as evidenced in pOXI1::GUS analysis, which showed strong expression along the vascular system (Fig. 1c) and was also reflected by the localized accumulation of ROS (Fig. 1d) and cell death (Fig. 1e) as evidenced by diamine benzidine (DAB) and trypan blue staining, respectively.
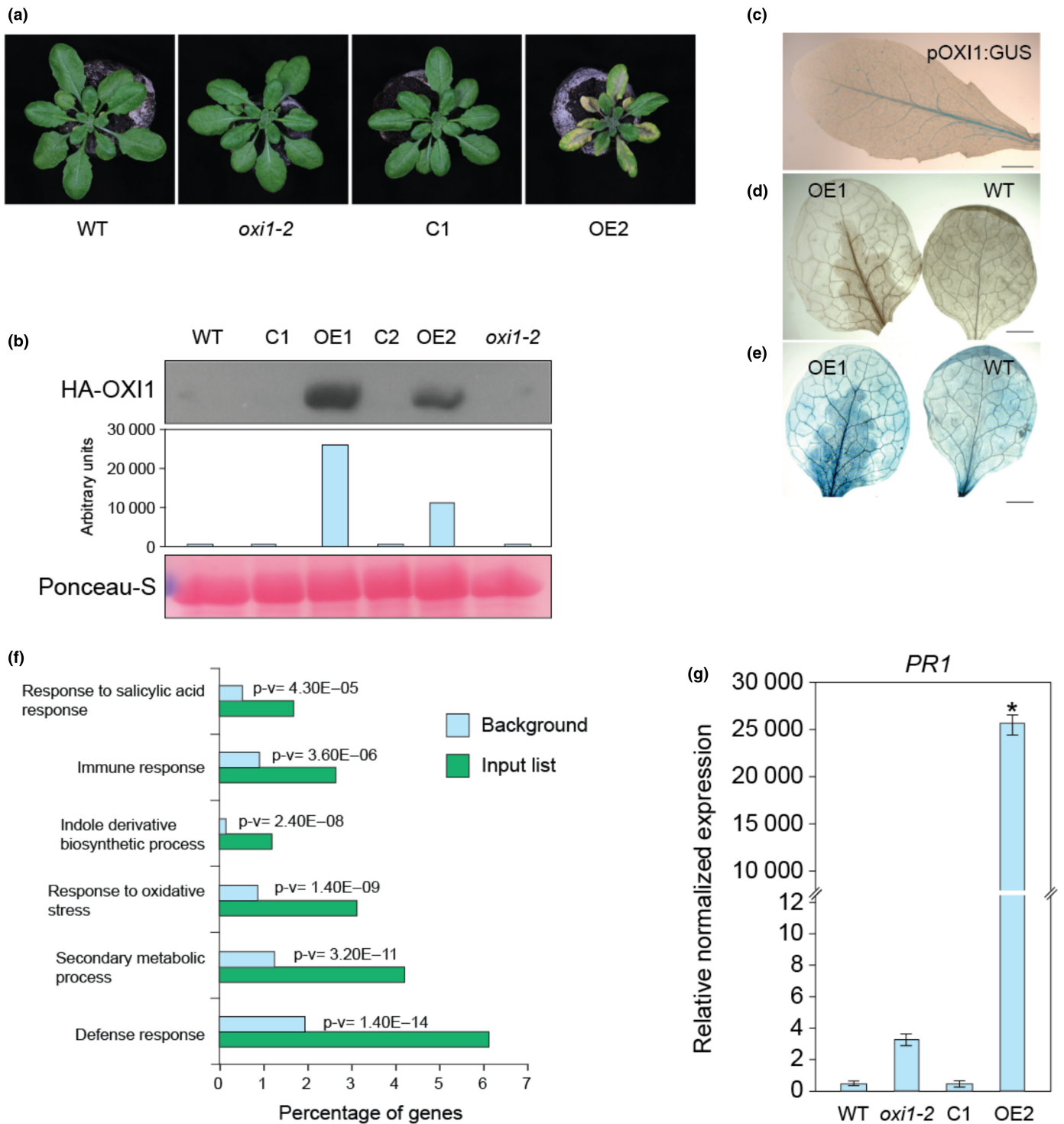
Fig. 1 *OXI1* regulates ROS, cell death, and defense-related genes. (a) Phenotypes of *Arabidopsis thaliana* Col-0 WT, *oxi1-2*, *C1*, and *OE2* plants grown for 4 wk on soil. (b) Western blot of 4-wk-old Col-0 WT, *C1*, *OE1*, *C2*, *OE2*, and *oxi1-2* plants with HA antibody. The bottom panel represents small ribulose bisphosphate carboxylase (Rbcs) staining by Ponceau S. (c) GUS staining of 4-wk-old leaf of *pOXI1::GUS* plant. Bar, 1 mm. (d) Diaminobenzidine staining for H_2O_2 in leaves of 4-wk-old *OE1* and Col-0 WT plants. Bar, 1 mm. (e) Trypan blue staining of leaves of 4-wk-old *OE1* and Col-0 WT plants. Bar, 1 mm. (f) GO analysis of significantly upregulated genes ($\log_2$(FC) ($P < 0.05$)) of 4-wk-old *OE2* when compared with Col-0 WT plants. Gene ontology term analysis was performed using the AGRIGO database (for a complete list of differentially regulated genes, see Table S4). (g) qRT-PCR of PR1 gene expression levels of Col-0 WT, *oxi1-2*, *C1*, and *OE2* in three independent experiments after normalization to actin ($n = 6$). Values represent the mean ± SE, * indicates significant difference from WT, $P \leq 0.05$, as determined by Student's *t*-test.

Transcriptome analysis of *OXI1* lines

To obtain insight into the underlying molecular processes giving rise to the cell death GOF phenotype in the *OXI1* overexpression lines, we performed a global transcriptome analysis of three *OXI1-OE* lines. Compared with Col-0, these lines showed 1055 upregulated genes (fold change $\geq$ 2) and 1004 downregulated genes (fold change $\leq$ 2) (Table S4). A gene ontology (GO) analysis of the upregulated genes revealed a significant overrepresentation of genes involved in metabolic and immune-related processes (Fig. 1f). For metabolic processes, mostly secondary metabolic pathways, such as amino acid- and indole-derivative biosynthetic processes, were induced (Fig. 1f; Table S4). Moreover, ion homeostasis, defense, SA, and JA pathways were significantly upregulated for the immune-related processes (Fig. 1f; Table S4), and PR1 gene expression levels were strongly enhanced upon overexpression of *OXI1* (Fig. 1g).

Proteome analysis of *OXI1* lines

In order to understand the changes induced by *OXI1* at the protein level, we carried out whole proteome analysis of WT, *oxi1-2*, *C1*, and *OE2* lines by LC–MS/MS of 4-wk-old plants. Proteomes of all the lines from four independent biological replicates were analyzed (Table S5). Proteins were considered to be differentially expressed with a $\log_2$ ratio of $> \pm 1$ and FDR < 0.05. Eighty-eight proteins were upregulated and 12 downregulated in WT compared with *OE2* as visualized in the volcano plot (Fig. 2a). Enrichment analysis was made using AGRIGO followed by removal of redundant GO terms using REVIGO. The comparison of OE2 with WT showed 88 upregulated proteins involved in defense response, innate immune response, and SAR (Fig. 2a). The 12 downregulated proteins showed no enrichment in GO terms. These data are consistent with the role of *OXI1* as a positive regulator of defense and cell death. Next, we compared *oxi1-2* with *OE2* (Fig. 2b). One hundred and forty proteins were enriched in the GO terms defense response, programmed cell death, and SAR (Fig. 2b). The 37 upregulated proteins in *oxi1-2* did not show any significant GO terms. Finally, on comparing *oxi1-2* with *C1*, the 23 downregulated proteins in *oxi1-2* did not show any significant GO terms, but the 122 upregulated proteins in *oxi1-2* belonged to the GO terms photosynthesis, photosynthesis light reaction, and oxidation–reduction process (Fig. 2c).

To test whether *OXI1* regulates the photosynthesis proteome at the level of transcription, we performed qRT-PCR on a number of photosynthesis genes. As shown in Fig. 2d, in comparison with WT and the *C1* complementation line, these photosynthesis-related genes show enhanced expression in *oxi1-2* but all of them were strongly repressed in *OE2*. In summary, these results are consistent with a negative role of *OXI1* in photosynthesis and metabolism.

### *OXI1* induces salicylic acid biosynthesis and SA responses

The transcriptome analysis suggested that *OXI1* regulates SA biosynthesis. Isochorismate synthase ICS1 also known as SID2 (SA-INDUCTION-DEFICIENT2) is the key enzyme for SA biosynthesis (Wildermuth *et al.*, 2001), transcript levels of which strongly accumulated in *OE2* (Fig. 3a,b). SA-INDUCTION-DEFICIENT2 expression is redundantly regulated by the transcription factors *Cbp60g* and *SARD1* (Zhang *et al.*, 2010), which were both found to be upregulated in *OXI1* overexpression lines (Fig. 3a, b). To quantify the levels of free SA, SA-β-glucoside (SAG), and SA glucose ester (SGE) upon pathogen challenge, we infected 4-wk-old Arabidopsis Col-0 WT, *oxi1-2*, *C1*, and *OE2* plants with *Psm*. In contrast to *oxi1-2*, which showed enhanced susceptibility, *OE2* showed enhanced resistance toward *Psm* when compared with WT or *C1* plants (Fig. 4a). Constitutive accumulation of all of SA, SAG, and SGE were found in *OE2* already in the absence of pathogen challenge (Figs 3c, S2). In addition, the levels of free and total SA (i.e. the sum of SA, SAG, and SGE) increased to similar levels in WT, *oxi1-2*, and the *C1* complementation line in response to *Psm* inoculation, at 10, 20, and 48 hpi. Interestingly, *OE2* was also primed for enhanced SA production in the earlier phases of the *Psm* interaction, which manifested itself in strongly enhanced levels of SAG, SGE, and total SA at 10 and 20 hpi (Figs 3c, S2). While WT, *oxi1-2*, and *C1* showed a systemic increase in SA, SAG, and SGE at 48-h post-*Psm* inoculation, the high constitutive levels of the three SA forms were not further increased in the systemic leaves of pathogen-challenged *OE2* (Figs 3c, S2). Overall, these results indicate that *OXI1* overexpression already poised plants for maximal SA synthesis before pathogen attack.

Salicylic acid signaling is mediated by the transcriptional regulator NPR1 which can shuttle from the cytoplasm to the nucleus in a redox-dependent manner and is dependent on the thioredoxins TRX-h3 and h5 (Tada *et al.*, 2008). Nuclear NPR1 then associates with TGA transcription factors to induce SA-dependent genes (Mou *et al.*, 2003; Zhang *et al.*, 2003). Interestingly, *OXI1-OE* lines show strongly enhanced levels of TRX-h3 and TRX-h5 transcripts, suggesting that SA signaling might also be enhanced in these plants (Fig. 3a,b). A major part of *OXI1*-regulated genes are SA-responsive genes. The list (Table S4) includes multiple WRKY transcription factors (*WRKY18*, *40*, and *60*), PR genes (*PR1*, *PR2*, *PR3*, *PR4*, and *PR5*), and the metabolic enzymes *PBS3*, *BAP1*, and alpha-dioxygenase *DOX1*, which is involved in the protection against oxidative stress and cell death (De León *et al.*, 2002).

OXI1 enhances WRKY33 transcript levels and camalexin biosynthesis

The transcriptome analysis indicated that the transcription factor *WRKY33* and its direct downstream target *PAD3* are strongly upregulated in *OXI1* overexpression plants (Fig. 4b). Since *CYP79B2* and *PAD3* encode key enzymes for camalexin synthesis (Fig. 4c), we quantified camalexin levels in WT, *oxi1-2*, *C1*, and *OE2* (Fig. 4d). Camalexin levels were strongly induced in all plant lines at 20 hpi with *Psm*. Moreover, in mock-treated *OE2* plants, camalexin levels were elevated in the absence of pathogen inoculation. In addition, the pathogen-induced accumulation of camalexin was more pronounced in *OE2* than in the other lines under investigation at 20 hpi (Fig. 4d). Interestingly, we also
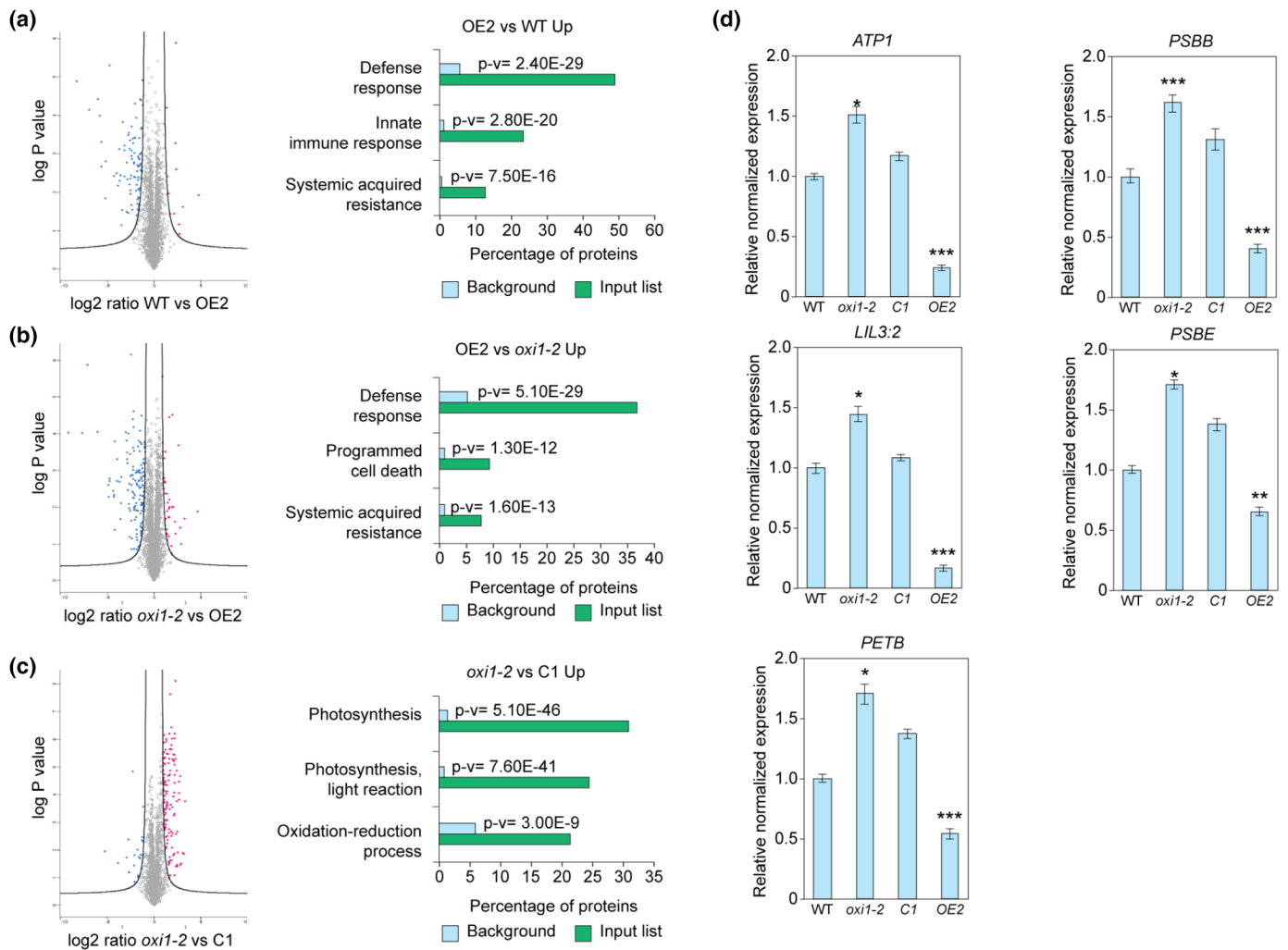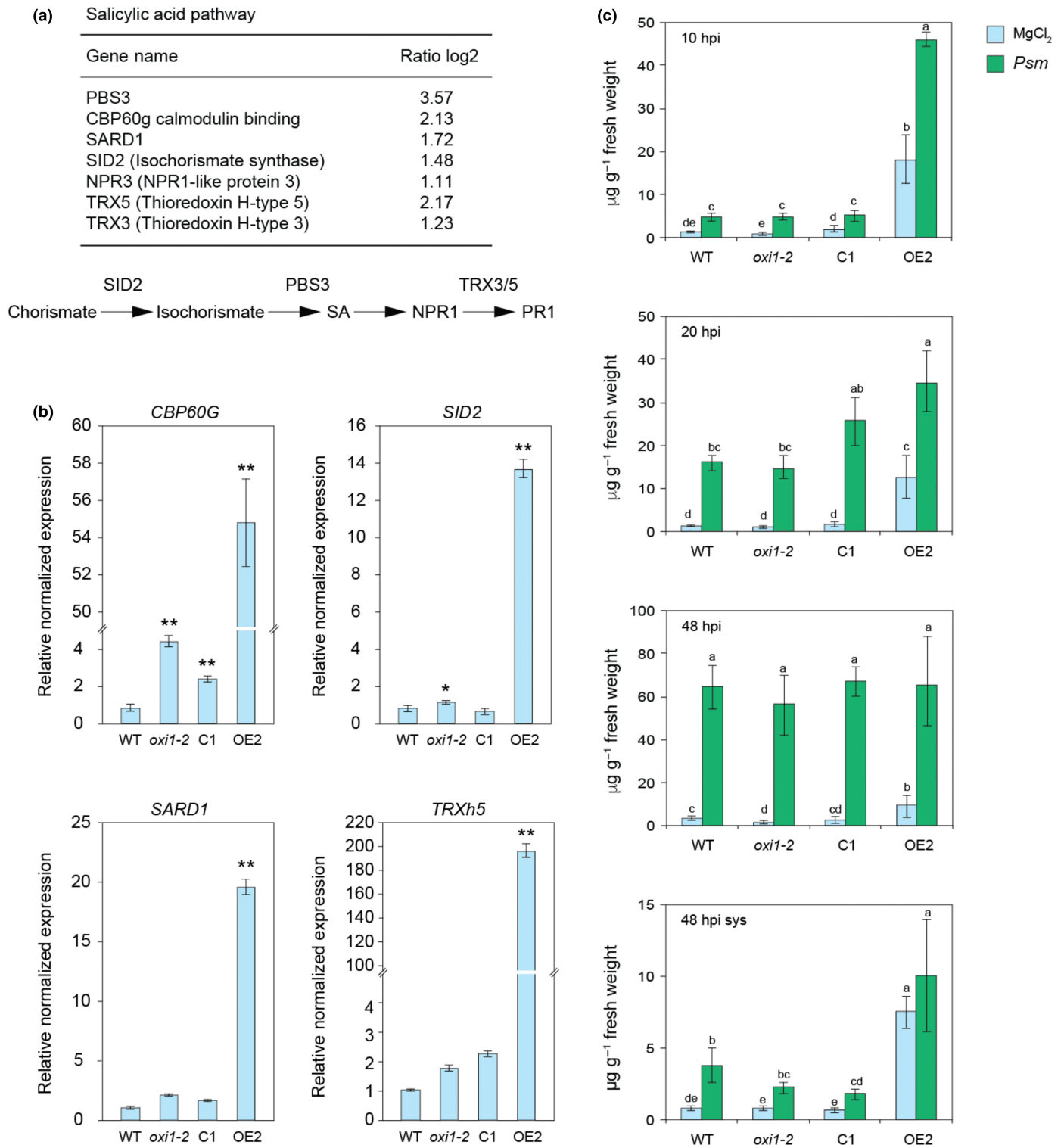
Fig. 2 Global proteome profile shows a role of *OXI1* in photosynthesis and defense responses. (a) Volcano plot depicting the differentially expressed proteins in *Arabidopsis thaliana* Col-0 WT vs OE2. Gene ontology enrichment of the downregulated proteins. (b) Volcano plot depicting the differentially expressed proteins in *oxi1-2* vs OE2. Gene ontology enrichment of the downregulated proteins. (c) Volcano plot depicting the differentially expressed proteins in *oxi1-2* vs *C1*. GO enrichment of the upregulated proteins. (a–c) The fold enrichment for the GO terms was calculated based on the frequency of proteins in the deregulated group compared with their frequency in the total proteome ($\log_2$ FC) ($P < 0.05$) using the AgriGo database (for complete protein lists see Table S5). (d) Gene expression of photosynthesis-related genes *ATP1*, *LIL1*, *PETB*, *PSBB*, and *PSBE* in 4-wk-old Col-0 WT, *oxi1-2*, *C1*, and *OE2* lines. qRT-PCR mean values in relation to WT of three independent experiments after normalization to actin $\pm$ SE ($n = 6$), * indicates significant difference from WT, $P \leq 0.05$, **, $P \leq 0.01$ as determined by Student's *t*-test.

observed strongly increased *CYP82C2* transcript levels in *OE2* plants (Fig. 4b). In contrast to *PAD3*, *CYP82C2* converts IAOx into 4-OH-ICN (Fig. 4c), another indolic compound with a key function in pathogen resistance (Rajniak *et al.*, 2015). In summary, these data show that *OXI1* activates the defense-related indolic pathway in Arabidopsis and strongly promotes the accumulation of the phytoalexin camalexin.

## *OXI1* triggers reactive oxygen species biosynthesis and homeostasis

Free radicals can be produced in Arabidopsis by several pathways, including from nitrous acid, which can be generated by at least two pathways upon pathogen attack. NO can be synthesized via

the nitrate reductases NIA1 and NIA2 or via an unknown mechanism by the GTPase NO-associated protein 1 (*AtNOA1*) (Lozano-Juste & León, 2010). In *OXI1* overexpressor lines, we found enhanced expression of *NIA2* (Table S4), suggesting that the lines might produce enhanced levels of NO. Reactive oxygen species and NO can both act as signaling molecules of free radicals and are both involved in pathogen defense. Upon pathogen infection of leaves, plants induce superoxide production via several means, including the NADPH oxidases *RbohD* and *RbohF* (Torres & Dangl, 2005). OXIDATIVE SIGNAL-INDUCIBLE1 GOF lines showed enhanced transcript levels of *RbohD* and *RbohF* (Fig. 5a,b) and accumulation of H_2O_2 (Fig. 5c). Moreover, a significant set of genes with roles in ROS homeostasis are identified in *OXI1-OE* lines, including ascorbate

(a) Salicylic acid pathway

Gene name	Ratio log2
PBS3	3.57
CBP60g calmodulin binding	2.13
SARD1	1.72
SID2 (Isochorismate synthase)	1.48
NPR3 (NPR1-like protein 3)	1.11
TRX5 (Thioredoxin H-type 5)	2.17
TRX3 (Thioredoxin H-type 3)	1.23

$$\text{Chorismate} \xrightarrow{\text{SID2}} \text{Isochorismate} \xrightarrow{\text{PBS3}} \text{SA} \rightarrow \text{NPR1} \xrightarrow{\text{TRX3/5}} \text{PR1}$$

Fig. 3 *OXI1* regulates SA biosynthesis, signaling, and basal immunity. (a) Selected upregulated genes related to SA biosynthesis in 4-wk-old *OE2* compared with *Arabidopsis thaliana* Col-0 WT plants. (b) *Cbp60g*, *SID2*, *SARD1*, and *TRXh5* gene expression levels in 4-wk-old Col-0 WT, *oxi1-2*, *C1* complementation, and *OE2* overexpression lines. qRT-PCR mean values in relation to Col-0 WT of three independent experiments after normalization to actin $\pm$ SE ($n = 6$), *, $P \leq 0.05$; **, $P \leq 0.01$ indicate significant differences from WT, as determined by Student's *t*-test. (c) Total levels of SA (sum of free SA, SAG, and SGE) in *Psm*-inoculated or mock-treated Arabidopsis leaves at 10, 20, and 48 hpi (hours postinfection), and in distal, systemic (sys) leaves at 48 hpi. Values $\pm$ SE are given in µg g^{-1} fresh weight ($n = 4$) of three independent experiments. Different letters above the bars denote statistically significant differences ($P < 0.05$, analysis of variance and *post hoc* Tukey's HSD test).

Fig. 4 *OXI1* controls basal immunity and camalexin biosynthesis. (a) Growth of *Psm* lux in 4-wk-old *Arabidopsis thaliana* Col-0 WT, *oxi1-2*, *C1*, and *OE2* plants. Bacterial numbers were assessed at 60 hpi (hours post infection) with the bioluminescent *Psm* lux strain and expressed as relative light units (rlu) per cm^2 leaf area. Data represent the mean $\pm$ SD of at least 20 leaf replicates ($n = 6$–7). Different letters denote significant differences ($P < 0.005$, analysis of variance and *post hoc* Tukey's HSD test). (b) Selected upregulated genes in 4-wk-old *OE2* plants related to (c) glucosinolate, camalexin, and 4-OH-ICN biosynthesis. Arrows denote enzymatic steps. Tryptophan (L-Trp); IAOx, indole-3-acetaldoxime; 4OH-ICN; ICY, indole-3-cyanohydrin; ANI, aci-nitro indole; 4-OH-ICN, 4-hydroxyindole-3-carbonylnitrile; I3M, indol-3-ylmethyl glucosinolate; ICN, indole-3-carbonylnitrile. (d) Camalexin levels in 4-wk-old Col-0 WT, *oxi1-2*, *C1*, and *OE2* lines upon infection with *Psm* at 10 and 20 hpi. Values $\pm$ SE are given in $\mu g\ g^{-1}$ fresh weight ($n = 4$) of three independent experiments. Different letters above the bars denote statistically significant differences ($P < 0.05$, analysis of variance and *post hoc* Tukey's HSD test). nd, nondetectable.
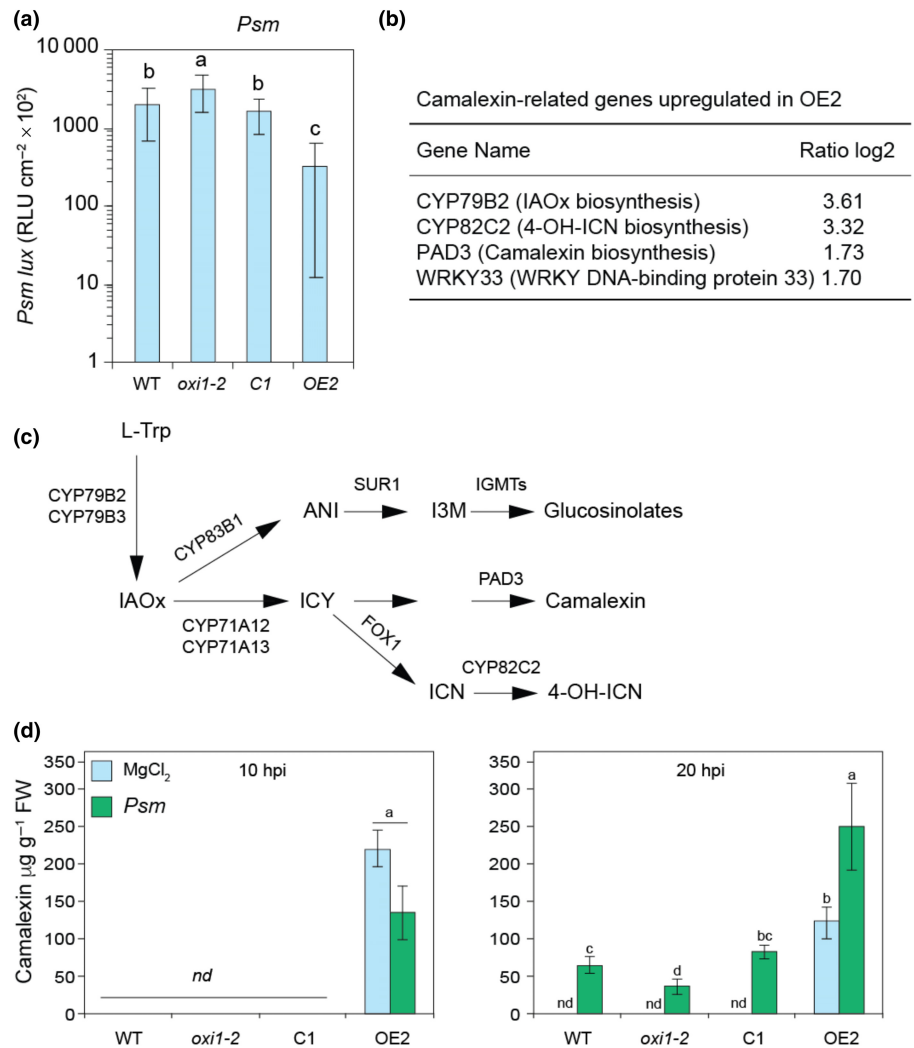
oxidase 1, the Cu/Zn superoxide dismutase *CSD1* (Fig. 5a), the oxidoreductase *TXR5*, or a number of peroxidases such as *PER32* or *PER50* (Table S4).

OXI1 induces polyamine biosynthesis gene expression

Polyamines play a role in plant growth, development, and in abiotic and biotic stress responses, including pathogen defense (Takahashi & Kakehi, 2010). In plants, putrescine is derived from arginine through several biosynthetic steps involving arginine decarboxylase (ADC), agmatine iminohydrolase (AIH), and N-carbamoylputrescine amidohydrolase (CPA) (Takahashi & Kakehi, 2010). In *OXI1* overexpressor plants, ADC gene expression levels were upregulated (Fig. 5d) and arginine and putrescine also accumulated (Figs 6, S3). Spermidine is synthesized from putrescine by spermidine synthase (SPDS) which requires decarboxylated S-adenosyl methionine (dc-SAM) as aminopropyl donor. Decarboxylated S-adenosyl methionine itself is derived from methionine by a two-step synthesis via S-adenosyl methionine synthase (SAMS) and S-adenosyl methionine decarboxylase

(SAMDC). Interestingly, both *OXI1* GOF lines did not show accumulation of spermidine in the metabolite profile, and SPDS, SAMS, and SAMDC transcript levels were downregulated (Table S4). Polyamines can also contribute to apoplastic H_2O_2 production by polyamine oxidases (PAO) (Moschou *et al.*, 2012). Therefore, it is also possible that some ROS in the *OXI1* GOF lines might be derived from polyamine oxidation reactions, although no upregulation of *PAO* gene expression levels was observed in any of the two lines.

OXI1 promotes basal resistance against virulent biotrophic pathogens

To verify the function of *OXI1* in basal resistance in the Col-0 accession, we spray-infected 4-wk-old Col-0 WT, *oxi1-2*, *C1*, and *OE2* with *Pst* DC3000 and determined bacterial proliferation levels at 3 dpi. In contrast to the *oxi1-2* mutant plants, which showed enhanced susceptibility, *OE2* showed enhanced resistance toward *Pst* DC3000 (Fig. 5e). In summary, the observed phenotypes correlate well with the function of *OXI1*
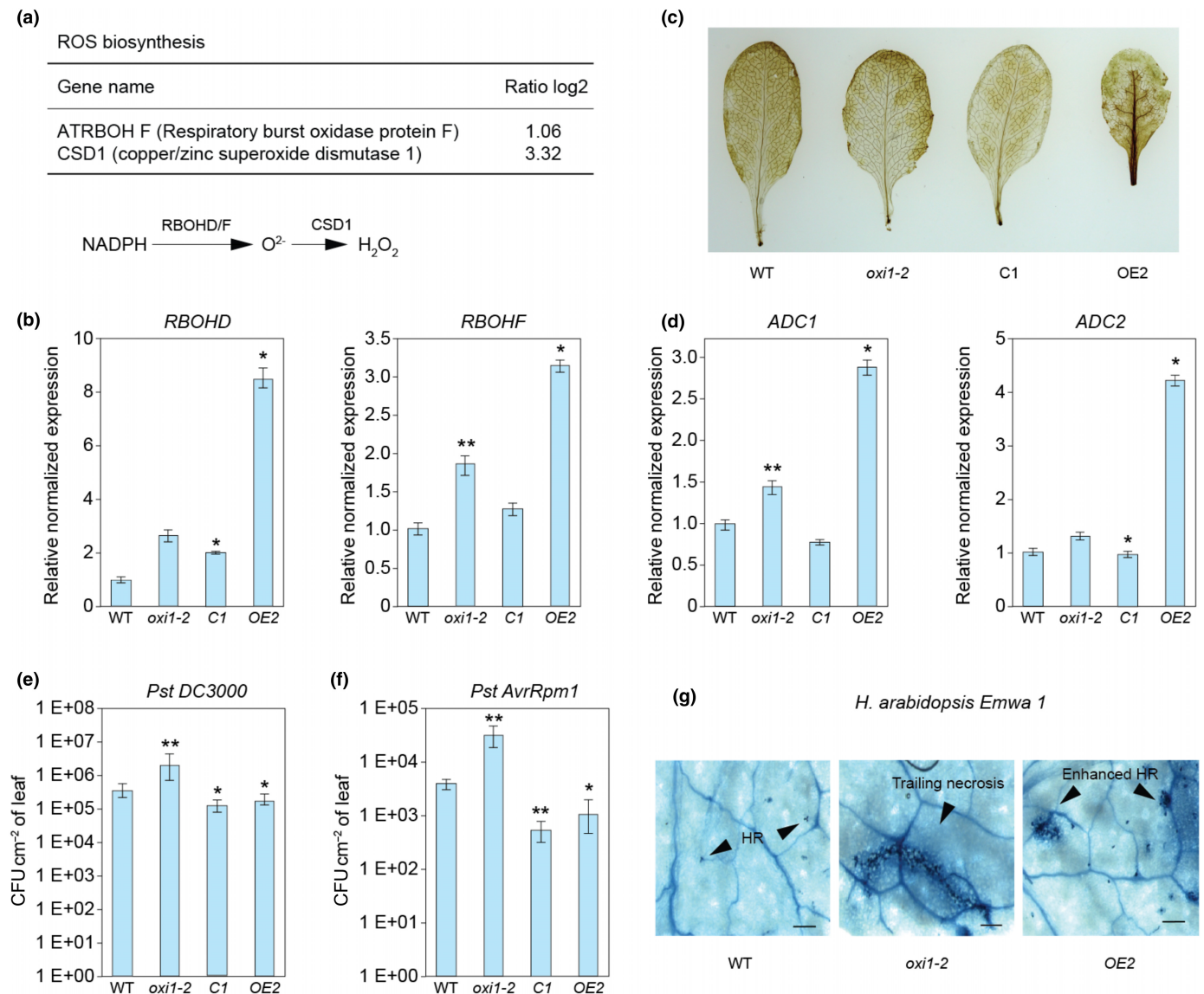
Fig. 5 *OXI1* triggers ROS production and enhances basal and effector-triggered immunity. (a) Selected upregulated genes related to reactive oxygen species biosynthesis in *OE2* compared to *Arabidopsis thaliana* Col-0 wild-type (WT) plants. (b) *RBOHD* and *RBOHF* gene expression levels in 4-wk-old Col-0 WT, *oxi1-2*, *C1*, and *OE2* lines. qRT-PCR mean values in relation to WT of three independent experiments after normalization to actin ± SE ($n = 6$), *, significant difference from WT, $P \leq 0.05$, **, $P \leq 0.01$ as determined by Student's t-test. (c) Diaminobenzidine staining of H_2O_2 in 4-wk-old Col-0 WT, *oxi1-2*, *OE2*, and *C1* lines. (d) *ADC1* and *ADC2* expression in Col-0 WT, *oxi1-2*, *C1*, and *OE2* lines. qRT-PCR mean values in relation to Col-0 WT of three independent experiments after normalization to actin ± SE ($n = 6$), *, significant difference from WT, $P \leq 0.05$, as determined by Student's t-test. (e) Growth of *Pst* DC3000 and (f) *Pst* DC3000 *AvrRpm1* in 4-wk-old Col-0 WT, *oxi1-2*, *C1*, and *OE2* plants. Bacterial titers of *Pst* and *Pst AvrRpm1* were determined at 3 dpi by spray inoculation of plants. Bars represent the average of at least four independent replicate experiments, and error bars show SD ($n = 6$). *, $P < 0.05$ and **, $P < 0.01$ by Student's t-test. (g) Growth of *H. arabidopsidis* Emwa1 in 4-wk-old Col-0 WT, *oxi1-2*, and *OE2* plants. Cell death structures were stained in leaves with lactophenol trypan blue 6 d after *H. arabidopsidis* Emwa1 inoculation. Bar, 100 µm.

as positive regulator of defense genes and antimicrobial substances.

OXI1 positively affects effector-triggered immunity

We also investigated the role of *OXI1* in ETI responses in the Col-0 background. We spray-infected plants with the avirulent *Pst AvrRpm1* strain that induces ETI due to the presence of the CC-NB-LRR resistance gene *RPM1*. As shown in Fig. 5f, *oxi1-2* was compromised in resistance against the avirulent *Pst AvrRpm1*

strain that is recognized by the CC-NB-LRR R protein RPM1. By contrast, *C1* and *OE2* showed enhanced resistance against *Pst AvrRpm1* (Fig. 5f). Surprisingly, *C1* showed enhanced resistance against *Pst* DC3000 and *Pst AvrRpm1*, suggesting that even small enhancement of *OXI1* expression might be sufficient to trigger a primed defense state.

To test the role of *OXI1* susceptibility to the oomycete *Hyaloperonosopora parasitica*, in Col-0 plants, 2-wk-old WT, *oxi1-2*, and *OE2* were sprayed with *H. arabidopsis Emwa1* (Hpa Emwa1) (Fig. 5g). While a trailing necrosis phenotype in *oxi1-2*
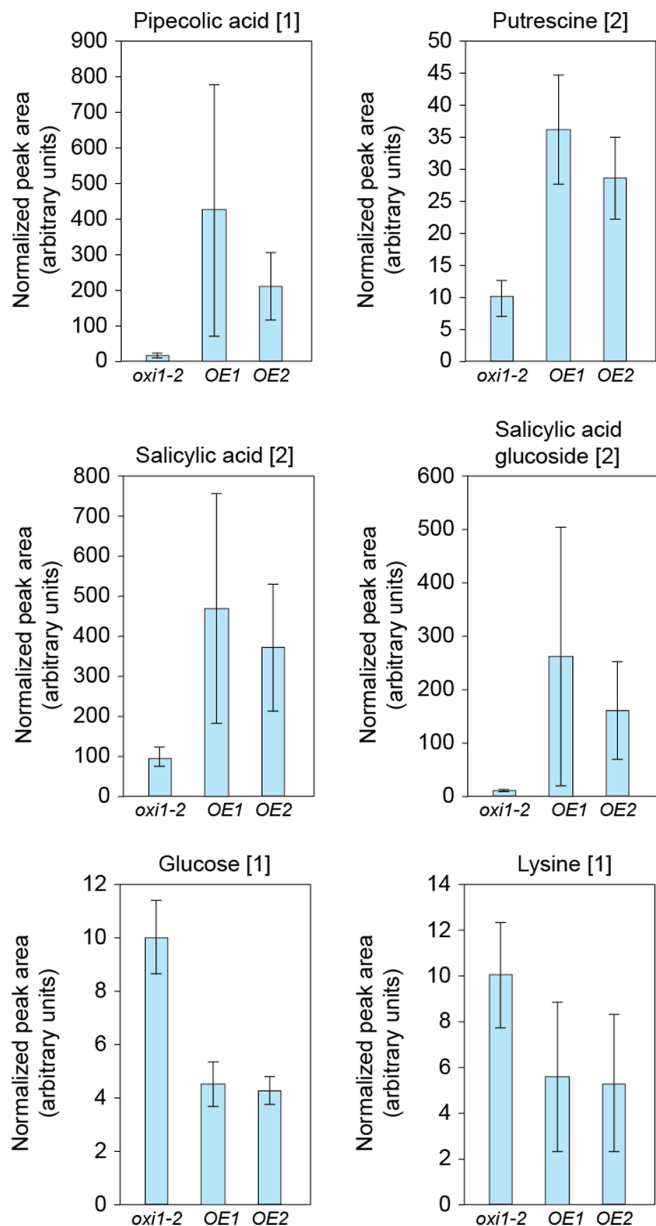
Fig. 6 *OXI1* regulation of metabolism. Global metabolite analysis was performed on 4-wk-old *Arabidopsis thaliana* Col-0 WT, *oxi1-2*, *OE1*, and *OE2* lines. Bar plots of pipecolic acid, putrescine, salicylic acid, salicylic acid glucoside, glucose and lysine (mean ± SD) representing normalized GC–MS peak areas in *oxi1-2*, *OE1*, and *OE2* compared with Col-0 WT (Mann–Whitney *U*-test, $P < 0.05$).

plants indicated enhanced susceptibility, HR at the infection sites of Col-0 plants correlated with their resistant phenotype, whereas *OE2* showed enhanced cell death spreading around infection sites. Overall, our results show that *OXI1* plays a role in ETI mediated by CC-NB-LRR resistance genes.

Metabolome analysis of *OXI1* reveals its function in regulating secondary metabolism

To further investigate the function of *OXI1*, we performed a global metabolomics analysis of *OE1*, *OE2*, and *oxi1-2* plants. In

comparison with the other lines including Col-0 WT plants, *oxi1-2* mutant plants showed only small differences in a number of metabolites. By contrast, both *OXI1-OE* lines showed very strong signatures, with several metabolites that accumulated compared with WT or decreased in *oxi1-2* mutant plants. Free SA or its glucoside were among the 10 most differentially accumulated metabolites in the *OXI1-OE* lines (Figs 6, S3). Interestingly, the most differently accumulated metabolite was pipecolic acid (Figs 6, S3), whose accumulation is required for local and systemic defense responses in Arabidopsis (Návarová *et al.*, 2012). We also found major differences in tyrosine, tryptophan, and the branched chain amino acids leucine, isoleucine, and valine, all of which are marker metabolites during a localized pathogen infection (Zeier, 2013). On the contrary, *OXI1-OE* lines showed lower levels of glucose and fructose and the amino acids lysine, proline, glycine, and glutamine when compared to WT plants (Figs 6, S3).

OXI1 regulates pipecolic acid and N-hydroxypipecolic acid biosynthesis

Accumulation of Pip is necessary for local and systemic defense responses in Arabidopsis. Pipecolic acid is derived from the amino acid lysine, whose levels were depleted in *OXI1* overexpression lines. The transaminase ALD1 converts L-Lys to 2,3-dehydropipecolic acid which is then reduced to Pip by SARD4 (Ding *et al.*, 2016; Hartmann *et al.*, 2017). Finally, Pip can be hydroxylated to NHP by FMO1 (Chen *et al.*, 2018; Hartmann *et al.*, 2018). N-hydroxypipecolic acid is the actual immune-active and SAR-inducing signal of this pathway (Hartmann & Zeier, 2019; Zeier, 2021). Upon pathogen attack, *ALD1*, *SARD4*, and *FMO1* are strongly upregulated and mutants in any of these genes show enhanced susceptibility to biotrophic pathogens (Song *et al.*, 2004; Mishina & Zeier, 2006; Hartmann *et al.*, 2017). In accordance with the transcriptome and metabolite data, *ALD1*, *SARD4*, and *FMO1* transcripts (Fig. 7a,b), and Pip and NHP metabolite levels accumulated already in mock-treated *OE2* plants without pathogen attack (Fig. 7c). Upon inoculation with *Psm*, Pip and NHP strongly accumulated in WT, *oxi1-2*, *C1*, and *OE2* plants from 10 hpi onward (Fig. 7c). Besides their constitutively enhanced Pip and NHP levels, *OE2* plants showed a primed biosynthesis of Pip and NHP, both at the sites of *Psm* infection (at 10 hpi for Pip, at 20 hpi for NHP) and in distal leaves (48 hpi) (Fig. 7c). These results indicate that *OXI1* promotes the biosynthesis of Pip and NHP via the transcriptional upregulation of *ALD1*, *SARD4*, and *FMO1*.

To test whether the enhanced resistance phenotype of *OXI1*-overexpressing plants is mediated by NHP, we crossed the *OXI1-OE* line *OE2* with *ald1* or *fmo1*, respectively. Remarkably, the strong pathogen resistance phenotype of *OE2* was completely suppressed in homozygous *OE2 ald1* and *OE2 fmo1* lines (Fig. 8a), indicating that the NHP pathway is essential for *OXI1* function in immunity.

We next verified that the enhanced NHP levels in *OE2* plants were fully dependent on *ALD1* and *FMO1* (Fig. 8b). As expected, the constitutive accumulation of Pip was completely
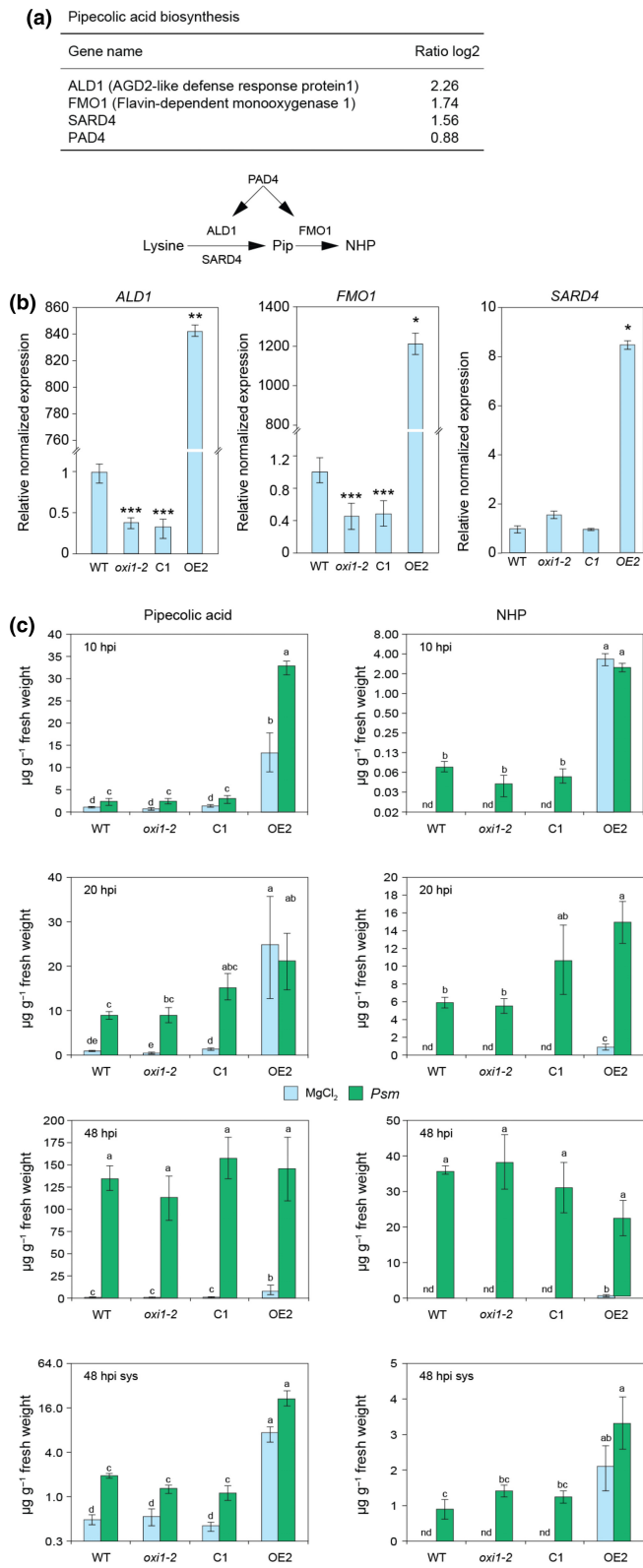
Fig. 7 *OXI1* induces pipecolic acid and NHP biosynthesis. (a) Selected upregulated genes related to pipecolic acid (Pip) and N-hydroxypipecolic acid (NHP) biosynthesis in *OE2* compared with *Arabidopsis thaliana* Col-0 wild-type (WT) plants. (b) *ALD1*, *FMO1*, and *SARD4* gene expression levels in 4-wk-old Col-0 WT, *oxi1-2*, *C1*, and *OE2* lines. qRT-PCR mean values in relation to WT in three independent experiments after normalization to actin ± SE ($n = 6$), *, $P \leq 0.05$; **, $P \leq 0.01$; ***, $P \leq 0.001$ indicate significant differences from WT, as determined by Student's *t*-test. (c) Pipecolic acid levels (left) and NHP levels (right) in Psm-inoculated or mock-treated Arabidopsis leaves at 10, 20 and 48 hpi (hours postinfection), and in distal, systemic (sys) leaves at 48 hpi. Values ± SE are given in µg g⁻¹ fresh weight ($n = 4$) of three independent experiments. Different letters above the bars denote statistically significant differences ($P < 0.05$, analysis of variance and *post hoc* Tukey's HSD test). nd, nondetectable.

and thus confirms the existence of a positive feedback loop in the induction of the NHP biosynthetic pathway (Hartmann & Zeier, 2019). Moreover, these data confirm that Pip and NHP accumulation is promoted by *OXI1*-dependent regulation of *ALD1* and *FMO1*.

Since *OXI1-OE* lines show constitutive accumulation of SA, we also asked whether the SA accumulation promoted by *OXI1* occurs independently of the NHP pathway. As seen in Fig. 8(b), total SA levels are partially suppressed in *OE2 ald1* and *OE2 fmo1* lines under nontreated and mock-treated conditions. We also determined the levels of free and conjugated forms of SA, but these results (Fig. S4) did not reveal a different regulation than those seen for total SA (Fig. 8b). These data suggest that *OXI1*-induced activation of the NHP pathway directly controls SA accumulation. Upon pathogen challenge, however, an NHP-independent mechanism seems to drive SA accumulation, as all lines accumulated SA to similar levels under these conditions (Fig. 8b,c).

Finally, we also verified whether the constitutive camalexin accumulation in *OXI1* GOF lines is linked to the NHP pathway. Similar to the situation of SA, camalexin levels were partially suppressed in *OE2 ald1* and *OE2 fmo1* lines under nontreated and mock-treated conditions (Fig. 8b). These data suggest that *OXI1* regulation of the NHP pathway directly impinges on camalexin accumulation. Upon pathogen challenge, however, all lines accumulated camalexin to similar levels (Fig. 8b), suggesting that an NHP-independent mechanism drives camalexin accumulation under pathogen conditions.

Discussion

OXIDATIVE SIGNAL-INDUCIBLE1 protein kinase is activated by treatment of plants with cellulose or H_2O_2 and links the activation of MPK3/MPK6 to disease resistance (Rentel *et al.*, 2004; Petersen *et al.*, 2009) as well as to the beneficial interaction with the endosymbiotic fungus *Piriformospora indica* (Camehl *et al.*, 2011). Interestingly, the *OXI1* gene is also strongly induced at the transcriptional level by various abiotic and biotic conditions that are usually associated with the occurrence of accumulated ROS levels, such as high light or heavy metals (Smeets *et al.*, 2013; Beaugelin *et al.*, 2019). To gain more insight into the function of *OXI1* in plants, we generated a

suppressed in *OE2 ald1* plants (Fig. 8b). Moreover, *OE2 fmo1* lines showed strongly attenuated constitutive accumulation of Pip (Fig. 8b). This indicates that *OXI1*-promoted NHP biosynthesis positively regulates the biosynthesis of its precursor Pip,
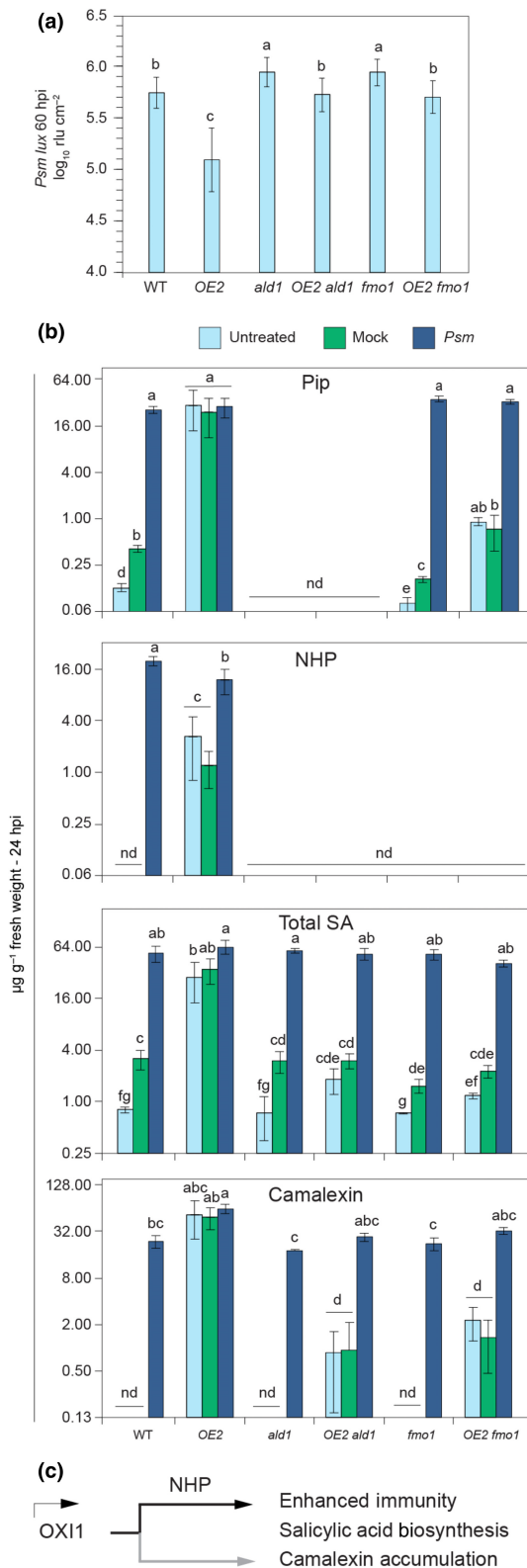
Fig. 8 Role of the NHP pathway in *OXI1*-induced basal resistance to virulent *Pseudomonas syringae*. (a) Naïve Arabidopsis of the indicated lines were inoculated with bioluminescent *P. syringae* pv *maculicola* ES4326 (*Psm*) expressing the *luxCDABE* operon from *Photorhabdus luminescens* (*Psm lux*) by syringe infiltration of three leaves each with a bacterial suspension of OD_{600} (optical density at 600 nm) = 0.001. As a measure of plant susceptibility, the numbers of bacteria were determined at 60 hpi (hours postinfection) in inoculated leaves by luminescence quantification and expressed as relative light units (rlu) per cm^2 leaf area (Gruner *et al.*, 2013). Bars indicate the mean ± SD of at least 15 leaf replicates ($n \geq 21$). Different letters denote significant differences ($P < 0.05$, analysis of variance and *post hoc* Tukey's HSD test). (b) Accumulation of defense-related metabolites in different Arabidopsis after bacterial inoculation. Levels (in µg g^{-1} fresh weight (FW)) of Pip, NHP, total SA (sum of free (unbound) SA, SA-β-glucoside (SAG) and SA glucose ester (SGE)), and camalexin in leaves inoculated with compatible *P. syringae* pv *maculicola* (*Psm*) at 24 hpi. The leaf metabolite levels of plants infiltrated with 10 mM $MgCl_2$ (mock) or of untreated plants (nt) harvested at the same time is also given. Bars represent means ± SD of four biological replicates ($n = 4$). One replicate sample consisted of four leaves from one plant. Different letters denote significant differences ($P < 0.05$, Kruskal–Wallis *H*-test). nd, not detected. (c) Model of *OXI1* mediated immunity. *OXI1* expression results in activation of the NHP pathway, thereby inducing SA and camalexin accumulation and pathogen resistance. A minor branch of OXI1-enhanced levels of SA, camalexin and immunity, is regulated by an NHP-independent branch.

4–5 wk of growth. These results are in contrast to those of Petersen *et al.* (2009) who generated *OXI1*-overexpressing lines under the 35S CaMV promoter in the Ws-2 background. Petersen *et al.* (2009) only reported one line and found no significant difference in the behavior of the *oxi1-1* knockout line in the Ws-2 background. By contrast, we observed that high *OXI1* levels are correlated with a GOF cell death phenotype in untreated plants and in basal and ETI. Although Petersen *et al.* (2009) detected *OXI1* transcripts in the Ws-2 line, *OXI1* protein was not measured. We previously also generated stable transgenic 35 S::*HA-OXI1* cDNA lines and in several of these lines we observed gene expression by qRT-PCR, but none of the lines had detectable OXI1 protein levels, indicating gene silencing and that constitutive expression of *OXI1* is not tolerated. We therefore generated HA-tagged *pOXI1::HA-OXI1* lines expressing the entire genomic *OXI1* locus. As shown in this work, coherent transcriptome, proteome, and metabolome analysis reveals a causal correlation of OXI1 protein levels with the GOF cell death and pathogen resistance phenotype and establishes *OXI1* as a positive regulator of programmed cell death and immunity.

Our metabolite analysis also revealed that *OXI1* promotes the accumulation of Pip and NHP, which are lysine-derived metabolites that have been shown to be essential components of SAR (Hartmann & Zeier, 2019). Pipecolic acid accumulates upon pathogen infection in both infected (local) and uninfected (distal) leaves (Hartmann *et al.*, 2017, 2018) and is generated by the chloroplast-localized lysine aminotransferase ALD1 and the dehydropipecolate reductase SARD4 (Ding *et al.*, 2016; Hartmann *et al.*, 2017). The importance of Pip in immunity is demonstrated in *ald1* mutants, which are compromised in pathogen-induced defense in both local and distal leaves (Song *et al.*, 2004; Návarová *et al.*, 2012). Interestingly, *OXI1-OE* plants show highly induced transcript levels of the key Pip

number of lines that express the genomic *OXI1* locus in the *oxi1-2* knockout background of Col-0. Aside from identifying weak expression lines that complement the *oxi1-2* phenotype, *OXI1* overexpression lines showed cell death phenotypes in plants after

biosynthesis enzymes *ALD1* and *SARD4*, suggesting that *OXI1* regulates Pip biosynthesis.

L-Pip is further hydroxylated to the SAR-activating metabolite NHP by *FMO1*. N-hydroxypipecolic acid biosynthesis by *FMO1* is induced at the transcriptional level by pathogens (Hartmann *et al.*, 2018), and our results suggested that *OXI1* triggers the accumulation of Pip and NHP via transcriptional upregulation of *ALD1* and *FMO1*. To test this hypothesis, we crossed *OE2* with *ald1* and/or *fmo1* to generate *OE2 ald1* and *OE2 fmo1* and compared Pip and NHP levels in these lines with those of WT, *ald1*, and *fmo1*. The constitutive and inducible accumulation of NHP in *OXI1-OE* lines was completely suppressed in *OE2 ald1* and *OE2 fmo1* under nontreated and mock-treated conditions, while Pip accumulation was fully blocked in *OE2 ald1* (Fig. 8b). This confirms that Pip and NHP accumulation under *OXI1*-overexpressing conditions is mediated by *ALD1* and *FMO1*, respectively. Interestingly, the *OXI1*-triggered accumulation of Pip is markedly attenuated in *OE2 fmo1* (Fig. 8b), indicating that Pip accumulation is promoted by NHP. This supports our previous hypothesis on the existence of a positive feedback loop in the NHP biosynthetic pathway (Hartmann & Zeier, 2019; Yildiz *et al.*, 2021; Zeier, 2021). Importantly, the enhanced pathogen resistance of *OXI1* overexpression lines was completely suppressed in homozygous *OE2 ald1* and *OE2 fmo1* lines (Fig. 8a). These results show that NHP functions as a main mediator of the here-described function of *OXI1* in plant immunity.

N-hydroxypipecolic acid induces the expression of a set of major plant immune genes to enhance defense readiness, amplifies resistance responses, acts synergistically with SA in the induction of SAR, promotes hypersensitive cell death, and primes plants for enhanced immune mobilization in cases of future pathogen challenge (Hartmann & Zeier, 2019). Pipecolic acid has also been shown to induce SA accumulation and the transcriptional induction of NHP biosynthetic genes in an FMO1-dependent manner, suggesting that elevated NHP levels trigger SA biosynthesis and amplify its own production (Bernsdorff *et al.*, 2016). In this context, hormone, metabolite, and chemical analysis indicated the strong accumulation of SA and its glucose-conjugated forms SAG and SGE upon *OXI1* expression at a time when the plants developed a cell death phenotype. Importantly, we could correlate these events with the expression of several genes involved in SA biosynthesis, such as *CBP60g* and *SARD1*, two key transcriptional regulators of *SID2* (Zhang *et al.*, 2010), encoding the isochorismate synthase enzyme responsible for SA biosynthesis (Wildermuth *et al.*, 2001). In agreement with upregulation of *CBP60g* and *SARD1*, *SID2* was equally upregulated and plants showed enhanced SA levels already in the absence of pathogen challenge.

The expression of the isochorismate synthase enzyme SID2 is strongly upregulated in *OXI1* overexpression lines (Fig. 3a,b) and the plants accumulate high levels of salicylic acid (Figs 3c, S2) and show enhanced cell death during development. Programmed cell death in plants is dependent on the accumulation of SA. To test whether the cell death phenotype of *OXI*1 GOF lines is dependent on SA, we crossed *OE2* with *sid2* mutants, which are compromised in SA biosynthesis. *OE2 sid2* plants partially suppressed the dwarf and cell death phenotype of the *OXI1-OE* line (Beaugelin *et al.*, 2019), indicating that *OXI1* regulates cell death by controlling the expression of the SA biosynthetic pathway.

Our data suggest that activation of *OXI1* results in NHP and SA production. Our results show that the *OXI1*-driven activation of SA biosynthesis is dependent on NHP (Fig. 8). These data support the existence of an NHP- and SA-dependent self-amplification machinery operating during the establishment of plant SAR (Zeier, 2021). Elevated NHP levels are causative for a primed state in plants (Yildiz *et al.*, 2021), and this is further confirmed by the potentiated NHP, SA, and camalexin accumulation in *OXI1-OE* plants following *Psm* attack. OXIDATIVE SIGNAL-INDUCIBLE1 belongs to the most highly and fastest induced Arabidopsis genes and proteins that react to a variety of stress conditions including pathogen attack (Rentel *et al.*, 2004). Our work here shows that *OXI1* plays a central role in the production of NHP, SA, and camalexin together contributing to enhanced innate immunity (Fig. 8c). However, recent work suggests that NHP is not upstream of SA, but acts in parallel to mutually amplify each other (Sun *et al.*, 2020). Interestingly, the analysis of *OE2 ald1* and *OE2 fmo1* lines suggests that *OXI1* also regulates an NHP-independent smaller signaling branch to contribute to SA accumulation (Fig. 8c). To further clarify the complex fine regulation, it will be interesting to investigate whether *OE2 sid2* plants are not affected in the upregulation of NHP levels.

In addition to NHP and SA, our data show that OXI1 is also a key regulator of ROS accumulation and signaling in Arabidopsis. The interaction of ROS with SA in immunity has been well-documented (Herrera-Vásquez *et al.*, 2015), but little knowledge exists yet on the link between ROS and NHP. One component that could be a common denominator linking ROS to SA is glutathione, as demonstrated for NPR1, which thereby acts as a cellular redox sensor (Mou *et al.*, 2003). Our transcriptome and metabolome analysis also indicated that *OXI1* activates the defense-related indolic pathway and strongly promotes camalexin accumulation. Glutathione might not only be linking ROS to SA but also to camalexin biosynthesis as γ-glutamyl cyclotransferase mutants of the defense-related indole pathway not only inhibit camalexin synthesis but also NHP and SA biosynthesis (Wang *et al.*, 2022). However, a number of other reports (Návarová *et al.*, 2012; Bernsdorff *et al.*, 2016; Hartmann *et al.*, 2018; Yildiz *et al.*, 2021) demonstrate that enhanced NHP levels prime for enhanced camalexin biosynthesis are consistent with the metabolic phenotypes of the *OXI1-OE2*, the *OXI1-OE2 fmo1*, and the *OXI1-OE2 ald1* lines (Fig. 8b). Overall, our results indicate that *OXI1* is at the heart of the regulation of a number of key factors of plant immunity and that further experiments are warranted to uncover the full complexity of *OXI1* functioning in defense.

Acknowledgements

Author contributions

CF generated and analyzed transgenic lines. MH performed pathogen assays. RL performed global metabolome analysis. MH, LA, SR and JZ analyzed selected metabolites. AAR and NR performed transcript analysis. AH, SCS, NR and HN performed the proteome analysis. JZ and HH designed the work and wrote the paper. AAR and MH contributed equally to this work.

Competing interests

None declared.

ORCID

Michael Hartmann (ID) https://orcid.org/0000-0003-4828-958X
Anne Harzen (ID) https://orcid.org/0000-0001-7370-4939
Heribert Hirt (ID) https://orcid.org/0000-0003-3119-9633
Hirofumi Nakagami (ID) https://orcid.org/0000-0003-2569-7062
Anamika A. Rawat (ID) https://orcid.org/0000-0001-9081-3547
Naganand Rayapuram (ID) https://orcid.org/0000-0003-2056-3735
Sara Christina Stolze (ID) https://orcid.org/0000-0002-1421-9703
Jürgen Zeier (ID) https://orcid.org/0000-0002-8703-5403

Data availability

The proteome data that support the findings of this study are openly available in PRIDE under the following project number PXD023853. Microarray data were deposited at CATdb (http://urgv.evry.inra.fr/cgi-bin/projects/CATdb/consult_expce.pl?experiment_id=337) (Project AU2010-01_OXI1) and GEO (Project GSE35941) according to the 'Minimum Information About a Microarray Experiment' standards. Global proteome sample preparation, data acquisition, and analysis by LC–MS/MS (Methods S2).

References

Alhoraibi H, Bigeard J, Rayapuram N, Colcombet J, Hirt H. 2019. Plant immunity: the MTI-ETI model and beyond. *Current Issues in Molecular Biology* 30: 39–58.

Apel K, Hirt H. 2004. Reactive oxygen species: metabolism, oxidative stress, and signal transduction. *Annual Review of Plant Biology* 55: 373–399.

Beaugelin I, Chevalier A, D'Alessandro S, Ksas B, Novák O, Strnad M, Forzani C, Hirt H, Havaux M, Monnet F. 2019. OXI1 and DAD regulate light-induced cell death antagonistically through Jasmonate and salicylate levels. *Plant Physiology* 180: 1691–1708.

Bernsdorff F, Döring AC, Gruner K, Schuck S, Bräutigam A, Zeier J. 2016. Pipecolic acid orchestrates plant systemic acquired resistance and defense priming via salicylic acid-dependent and -independent pathways. *Plant Cell* 28: 102–129.

Berriri S, Garcia AV, Frei dit Frey N, Rozhon W, Pateyron S, Leonhardt N, Montillet JL, Leung J, Hirt H, Colcombet J. 2012. Constitutively active mitogen-activated protein kinase versions reveal functions of *Arabidopsis* MPK4 in pathogen defense signaling. *Plant Cell* 24: 4281–4293.

Bigeard J, Colcombet J, Hirt H. 2015. Signaling mechanisms in pattern-triggered immunity (PTI). *Molecular Plant* 8: 521–539.

Camehl I, Drzewiecki C, Vadassery J, Shahollari B, Sherameti I, Forzani C, Munnik T, Hirt H, Oelmüller R. 2011. The OXI1 kinase pathway mediates Piriformospora indica-induced growth promotion in Arabidopsis. *PLoS Pathogens* 7: e1002051.

Caplan J, Padmanabhan M, Dinesh-Kumar SP. 2008. Plant NB-LRR immune receptors: from recognition to transcriptional reprogramming. *Cell Host & Microbe* 3: 126–135.

Carbon S, Ireland A, Mungall CJ, Shu S, Marshall B, Lewis S, the AmiGO Hub, the Web Presence Working Group. 2008. AMiGO: online access to ontology and annotation data. *Bioinformatics* 25: 288–289.

Castro B, Citterico M, Kimura S, Stevens DM, Wrzaczek M, Coaker G. 2021. Stress-induced reactive oxygen species compartmentalization, perception and signalling. *Nature Plants* 7: 403–412.

Chen Y-C, Holmes EC, Rajniak J, Kim J-G, Tang S, Fischer CR, Mudgett MB, Sattely ES. 2018. *N*-hydroxy-pipecolic acid is a mobile metabolite that induces systemic disease resistance in *Arabidopsis. Proceedings of the National Academy of Sciences, USA* 115: E4920–E4929.

Chinchilla D, Zipfel C, Robatzek S, Kemmerling B, Nürnberger T, Jones JDG, Felix G, Boller T. 2007. A flagellin-induced complex of the receptor FLS2 and BAK1 initiates plant defence. *Nature* 448: 497–500.

De León IP, Sanz A, Hamberg M, Castresana C. 2002. Involvement of the Arabidopsis alpha-DOX1 fatty acid dioxygenase in protection against oxidative stress and cell death. *The Plant Journal* 29: 61–62.

DeFalco TA, Zipfel C. 2021. Molecular mechanisms of early plant pattern-triggered immune signaling. *Molecular Cell* 81: 3449–3467.

Ding P, Rekhter D, Ding Y, Feussner K, Busta L, Haroth S, Xu S, Li X, Jetter R, Feussner I *et al.* 2016. Characterization of a pipecolic acid biosynthesis pathway required for systemic acquired resistance. *Plant Cell* 28: 2603–2615.

Fan J, Crooks C, Lamb C. 2008. High-throughput quantitative luminescence assay of the growth in planta of *Pseudomonas syringae* chromosomally tagged with *Photorhabdus luminescens luxCDABE. The Plant Journal* 53: 393–399.

Forzani C, Carreri A, de la Fuente van Bentem S, Lecourieux D, Lecourieux F, Hirt H. 2011. The Arabidopsis protein kinase Pto-interacting 1-4 is a common target of the oxidative signal-inducible 1 and mitogen-activated protein kinases. *The FEBS Journal* 278: 1126–1136.

Frei dit Frey N, Garcia AV, Bigeard J, Zaag R, Bueso E, Garmier M, Pateyron S, de Tauzia-Moreau ML, Brunaud V, Balzergue S *et al.* 2014. Functional analysis of Arabidopsis immune-related MAPKs uncovers a role for MPK3 as negative regulator of inducible defences. *Genome Biology* 15: R87.

Gómez-Gómez L, Boller T. 2000. FLS2: an LRR Receptor–like kinase involved in the perception of the bacterial elicitor flagellin in *Arabidopsis. Molecular Cell* 5: 1003–1011.

Gruner K, Griebel T, Návarová H, Attaran E, Zeier J. 2013. Reprogramming of plants during systemic acquired resistance. *Frontiers in Plant Science* 4: 252.

Hartmann M, Kim D, Bernsdorff F, Ajami-Rashidi Z, Scholten N, Schreiber S, Zeier T, Schuck S, Reichel-Deland V, Zeier J. 2017. Biochemical principles and functional aspects of pipecolic acid biosynthesis in plant immunity. *Plant Physiology* 174: 124–153.

Hartmann M, Zeier J. 2019. N-hydroxypipecolic acid and salicylic acid: a metabolic duo for systemic acquired resistance. *Current Opinion in Plant Biology* 50: 44–57.

Hartmann M, Zeier T, Bernsdorff F, Reichel-Deland V, Kim D, Hohmann M, Scholten N, Schuck S, Bräutigam A, Hölzel T *et al.* 2018. Flavin monooxygenase-generated N-hydroxypipecolic acid is a critical element of plant systemic immunity. *Cell* 173: 456–469.

Herrera-Vásquez A, Salinas P, Holuigue L. 2015. Salicylic acid and reactive oxygen species interplay in the transcriptional control of defense genes expression. *Frontiers in Plant Science* 6: 171.

Jeworutzki E, Roelfsema MR, Anschütz U, Krol E, Elzenga JT, Felix G, Boller T, Hedrich R, Becker D. 2010. Early signaling through the Arabidopsis pattern recognition receptors FLS2 and EFR involves Ca-associated opening of plasma membrane anion channels. *The Plant Journal* 62: 367–378.

Jones JDG, Dangl JL. 2006. The plant immune system. *Nature* 444: 323–329.

Kopka J, Schauer N, Krueger S, Birkemeyer C, Usadel B, Bergmüller E, Dörmann P, Weckwerth W, Gibon Y, Stitt M et al. 2005. GMD@CSB.DB: the Golm Metabolome Database. *Bioinformatics* 21: 1635–1638.

Ligterink W, Kroj T, zur Nieden U, Hirt H, Scheel D. 1997. Receptor-mediated activation of a MAP kinase in pathogen defense of plants. *Science* 276: 2054–2057.

Lozano-Juste J, León J. 2010. Enhanced abscisic acid-mediated responses in *nia1nia2noa1-2* triple mutant impaired in NIA/NR- and AtNOA1-dependent nitric oxide biosynthesis in Arabidopsis. *Plant Physiology* 152: 891–903.

Lurin C, Andrés C, Aubourg S, Bellaoui M, Bitton F, Bruyère C, Caboche M, Debast C, Gualberto J, Hoffmann B et al. 2004. Genome-wide analysis of Arabidopsis pentatricopeptide repeat proteins reveals their essential role in organelle biogenesis. *Plant Cell* 16: 2089–2103.

Mishina TE, Zeier J. 2006. The Arabidopsis flavin-dependent monooxygenase FMO1 is an essential component of biologically induced systemic acquired resistance. *Plant Physiology* 141: 1666–1675.

Moschou PN, Wu J, Cona A, Tavladoraki P, Angelini R, Roubelakis-Angelakis KA. 2012. The polyamines and their catabolic products are significant players in the turnover of nitrogenous molecules in plants. *Journal of Experimental Botany* 63: 5003–5015.

Mou Z, Fan W, Dong X. 2003. Inducers of plant systemic acquired resistance regulate NPR1 function through redox changes. *Cell* 113: 935–944.

Návarová H, Bernsdorff F, Döring AC, Zeier J. 2012. Pipecolic acid, an endogenous mediator of defense amplification and priming, is a critical regulator of inducible plant immunity. *Plant Cell* 24: 5123–5141.

Nawrath C, Métraux JP. 1999. Salicylic acid induction-deficient mutants of Arabidopsis express PR-2 and PR-5 and accumulate high levels of camalexin after pathogen inoculation. *Plant Cell* 11: 1393–1404.

Petersen LN, Ingle RA, Knight MR, Denby KJ. 2009. OXI1 protein kinase is required for plant immunity against *Pseudomonas syringae* in Arabidopsis. *Journal of Experimental Botany* 60: 3727–3735.

Pruitt RN, Gust AA, Nürnberger T. 2021. Plant immunity unified. *Nature Plants* 7: 382–383.

Rajniak J, Barco B, Clay NK, Sattely ES. 2015. A new cyanogenic metabolite in Arabidopsis required for inducible pathogen defence. *Nature* 525: 376–379.

Ranf S, Eschen-Lippold L, Pecher P, Lee J, Scheel D. 2011. Interplay between calcium signalling and early signalling elements during defence responses to microbe- or damage-associated molecular patterns. *The Plant Journal* 68: 100–113.

Rekhter D, Lüdke D, Ding Y, Feussner K, Zienkiewicz K, Lipka V, Wiermer M, Zhang Y, Feussner I. 2019. Isochorismate-derived biosynthesis of the plant stress hormone salicylic acid. *Science* 365: 498–502.

Rentel MC, Lecourieux D, Ouaked F, Usher SL, Petersen L, Okamoto H, Knight H, Peck SC, Grierson CS, Hirt H et al. 2004. OXI1 kinase is necessary for oxidative burst-mediated signalling in *Arabidopsis*. *Nature* 427: 858–861.

Ritchie ME, Phipson B, Wu D, Hu Y, Law CW, Shi W, Smyth GK. 2015. limma powers differential expression analyses for RNA-sequencing and microarray studies. *Nucleic Acids Research* 43: e47.

Smeets K, Opdenakker K, Remans T, Forzani C, Hirt H, Vangronsveld J, Cuypers A. 2013. The role of the kinase OXI1 in cadmium- and copper-induced molecular responses in *Arabidopsis thaliana*. *Plant, Cell & Environment* 36: 1228–1238.

Song JT, Lu H, McDowell JM, Greenberg JT. 2004. A key role for *ALD1* in activation of local and systemic defenses in *Arabidopsis*. *The Plant Journal* 40: 200–212.

Stahl E, Hartmann M, Scholten N, Zeier J. 2019. A role for tocopherol biosynthesis in Arabidopsis basal immunity to bacterial infection. *Plant Physiology* 181: 1008–1028.

Storey JD, Tibshirani R. 2003. Statistical significance for genomewide studies. *Proceedings of the National Academy of Sciences, USA* 100: 9440–9445.

Sumner LW, Amberg A, Barrett D, Beale MH, Beger R, Daykin CA, Fan TWM, Fiehn O, Goodacre R, Griffin JL et al. 2007. Proposed minimum reporting standards for chemical analysis. *Metabolomics* 3: 211–221.

Sun T, Huang J, Xu Y, Verma V, Jing B, Sun Y, Ruiz Orduna A, Tian H, Huang X, Xia S et al. 2020. Redundant CAMTA transcription factors negatively regulate the biosynthesis of salicylic acid and N-hydroxypipecolic acid by modulating the expression of SARD1 and CBP60g. *Molecular Plant* 13: 144–156.

Tada Y, Spoel SH, Pajerowska-Mukhtar K, Mou Z, Song J, Wang C, Zuo J, Dong X. 2008. Plant immunity requires conformational changes [corrected] of NPR1 via S-nitrosylation and thioredoxins. *Science* 321: 952–956.

Takahashi T, Kakehi J. 2010. Polyamines: ubiquitous polycations with unique roles in growth and stress responses. *Annals of Botany* 105: 1–6.

Torrens-Spence MP, Bobokalonova A, Carballo V, Glinkerman CM, Pluskal T, Shen A, Weng J-K. 2019. PBS3 and EPS1 complete salicylic acid biosynthesis from isochorismate in Arabidopsis. *Molecular Plant* 12: 1577–1586.

Torres MA, Dangl JL. 2005. Functions of the respiratory burst oxidase in biotic interactions, abiotic stress and development. *Current Opinion in Plant Biology* 8: 397–403.

Wang Z, Yang L, Jander G, Bhawal R, Zhang S, Liu Z, Oakley A, Hua J. 2022. AIG2A and AIG2B limit the activation of salicylic acid-regulated defenses by tryptophan-derived secondary metabolism in Arabidopsis. *Plant Cell* 34: 4641–4660.

Waszczak C, Carmody M, Kangasjärvi J. 2018. Reactive oxygen species in plant signaling. *Annual Review of Plant Biology* 69: 209–236.

Wildermuth MC, Dewdney J, Wu G, Ausubel FM. 2001. Isochorismate synthase is required to synthesize salicylic acid for plant defence. *Nature* 414: 562–565.

Yildiz I, Mantz M, Hartmann M, Zeier T, Kessel J, Thurow C, Gatz C, Petzsch P, Köhrer K, Zeier J. 2021. The mobile SAR signal N-hydroxypipecolic acid induces NPR1-dependent transcriptional reprogramming and immune priming. *Plant Physiology* 186: 1679–1705.

Zeier J. 2013. New insights into the regulation of plant immunity by amino acid metabolic pathways. *Plant, Cell & Environment* 36: 2085–2103.

Zeier J. 2021. Metabolic regulation of systemic acquired resistance. *Current Opinion in Plant Biology* 62: 102050.

Zeier J, Pink B, Mueller MJ, Berger S. 2004. Light conditions influence specific defence responses in incompatible plant-pathogen interactions: uncoupling systemic resistance from salicylic acid and PR-1 accumulation. *Planta* 219: 673–683.

Zhang Y, Tessaro MJ, Lassner M, Li X. 2003. Knockout analysis of Arabidopsis transcription factors *TGA2*, *TGA5*, and *TGA6* reveals their redundant and essential roles in systemic acquired resistance. *Plant Cell* 15: 2647–2653.

Zhang Y, Xu S, Ding P, Wang D, Cheng YT, He J, Gao M, Xu F, Li Y, Zhu Z et al. 2010. Control of salicylic acid synthesis and systemic acquired resistance by two members of a plant-specific family of transcription factors. *Proceedings of the National Academy of Sciences, USA* 107: 18220–18225.

Supporting Information

Additional Supporting Information may be found online in the Supporting Information section at the end of the article.

Fig. S1 Characterization of OXIDATIVE SIGNAL-INDUCIBLE1 (*OXI1*) lines.

Fig. S2 OXIDATIVE SIGNAL-INDUCIBLE1 (*OXI1*) regulation of SA biosynthesis.

Fig. S3 OXIDATIVE SIGNAL-INDUCIBLE1 (*OXI1*) regulation of metabolism.

Fig. S4 SA derivatives in different OXIDATIVE SIGNAL-INDUCIBLE1 (*OXI1*) Arabidopsis lines after mock- or *Pseudomonas syringae* pv *maculicola* inoculation.

Methods S1 GC–MS metabolomics.

Methods S2 Global proteome sample preparation, data acquisition, and analysis by LC–MS/MS.

Table S1 List of the 42 variables detected in Arabidopsis rosettes and identification parameters.

Table S2 GC–MS metabolomic raw data set: relative content of 42 metabolites in Arabidopsis leaves extracts (arbitrary unit: normalized peak area of integrated EICs).

Table S3 Nucleotide sequences for qRT-PCR analysis.

Table S4 Upregulated genes in Arabidopsis OXIDATIVE SIGNAL-INDUCIBLE1 (*OXI1*) lines.

Table S5 Proteome analysis of Arabidopsis OXIDATIVE SIGNAL-INDUCIBLE1 (*OXI1*) lines.

Please note: Wiley is not responsible for the content or functionality of any Supporting Information supplied by the authors. Any queries (other than missing material) should be directed to the *New Phytologist* Central Office.